Thermal properties and oil absorption behavior of TPU/natural fibers composites

N.A. Ahad*, N.F.H. Mohd Radzi, N.S. Sadli, J.S. Tan

School of Materials Engineering, Universiti Malaysia Perlis, Kompleks Pusat Pengajian Jejawi 2, 02600, Jejawi, Perlis, Malaysia

*Corresponding e-mail: norazwin@unimap.edu.my

Keywords: TPU; natural fibers; thermal properties

ABSTRACT - Natural fibers are usually selected as filler because it is readily available and environmentally friendly, inexpensive, non-toxic, biodegradable and still have good characteristics for a variety of uses. In this study, four types of natural fiber have been used which; coconut shell, coconut fiber, corn cob, and pineapple skin, as fillers in thermoplastic polyurethane (TPU). The mixing process conducted through melt mixing techniques. The percentage of TPU/natural fibers are 95/5, 90/10 and 85/15. Higher fiber loading will increase the thermal stability and it also depends on the type of fiber itself. Swelling testing is also having been done to prove the absorbency ability by natural fiber composites in cooking oil and engine oil. The pineapple fiber absorbed a large amount of both oil compared to others.

1. INTRODUCTION

The natural fibers are the one of popular resource that uses as reinforcement or filler in the polymer matrix [1] Coconut husk and shell powder, pineapple fiber and corn cob are some of the sources of natural fibers that have potential to use as filler, which has been studied here and blended with TPU. There are several recent studies that combined the natural fiber and TPU, found it to produce some of the unique properties. Many researchers have been studied natural fiber in polymer composites and it's mechanical, morphological properties in order to investigate the compatibility of fiber/polymer composites. Due to that, we investigated the effect of four types of natural fiber as filler in TPU, with different content of filler on thermal properties and the swelling percentage of the composite for the optimum content of filler in cooking oil and engine oil, to portray the issue of oil absorption by the composite of the four types of filler.

2. METHODOLOGY

Polymer-based TPU in the pallet form was supplied from Duplas Marketing Sdn. Bhd. All natural fibers (pineapple, coconut husk, coconut shell and corncob) were collected from market, stall and village. The dried fibers were grinded using grinding machine to produce fibers in the small size and were sieved using sieve shaker to get fine size between the ranges of 50 – 125 μm. The composite was prepared by melt blending technique using laboratory internal mixer at the weight percent of 95/5, 90/10 and 85/15 for TPU and natural fiber. Blending was carried out at temperature 180°C, with a mixing speed of 60 rpm for 10 min. The thermogravimetric analysis (TGA) was analyzed by using Metter Toledo TGA, from 27°C until 700°C with a heating rate of 10°C per min. Oil absorption test has been done to prove the ability of the composites to absorb cooking oil and engine oil. The test has been observed and determined for four weeks until equilibrium at room temperature. The samples were weighted for everyday and calculated using the equation of:

$$\text{Oil absorption} = \frac{\text{initial weight} - \text{final weight}}{\text{final weight}} \times 100\% \ (\%)$$

3. RESULTS AND DISCUSSION

In this study, for these two result (thermal properties and swelling percentage), we just consider for the TPU composites at optimum fiber loading from previous study [2]; which are 5% for pineapple fibers, 10% coconut husk, 10% for corn cob fibers and 15% for coconut shell. The observed data, $T_{10,}$ $T_{50,}$ and T_{90} for TPU/ natural fibers were shown in Table 1. As we can see, at T_{10} the degradation temperature of each composite is not significantly different, just different 1 to 7°C only. All composites decomposed hemicelluloses at this stage. For T_{50} and T_{90}, TPU/ coconut shell showed higher degradation temperatures compared to other composites. It shows the degradation at 50%, the stability of TPU / coconut shell is the highest. It may also be caused composite is filled 15% coconut shell.

Table 1 Observed data for TPU/natural fibers composites.

Fiber/%	T_{10} (°C)	T_{50} (°C)	T_{90} (°C)
Pineapple 5%	326	377	480
Coconut husk 10%	327	395	556
Corncob 10%	323	400	589
Coconut shell 15%	320	405	612

When the fiber content increased, thermal stability and degradation temperature also increased [3]. Also, the degradation temperature also related to the three stages degradation of the filler, which are consisting of hemicelluloses, cellulose and lignin, as well as

depending on the type of fibers and their chemical composition [4]. Low filler-matrix interaction also contributes to the thermal instability of the filled composite.

The pattern of oil absorption of TPU/natural fibers composites can be referenced in Fig. 1. All fibers showed higher oil absorption capacity for cooking oil compared to engine oil. Cooking oil has low viscosity so that the oil molecules can move easily to the pores of the fiber assembly and hence higher absorption capacity was observed. Several types of fibers have some drawback like oil absorption capacity due to its oleophobicity properties [5]. Other reasons are due to their shape, surface area and their nature. Strong fiber and matrix interfacial adhesion also can help to diminish the oil penetration and avoiding the worsening of the mechanical performance of the composite.

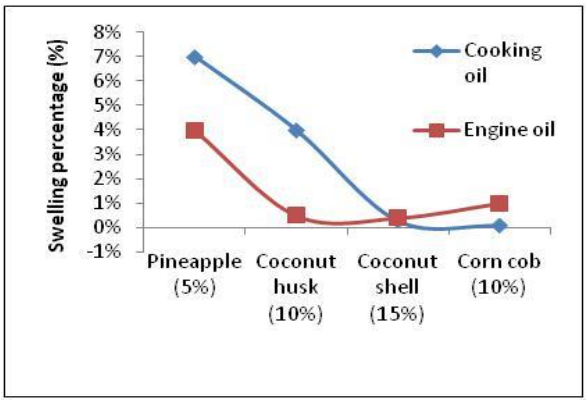

Figure 1 Swelling percentage for TPU/ natural fibers composites in cooking oil and engine oil after 4 weeks.

4. SUMMARY

TPU composite with higher fiber loading will increase the thermal stability and it also depends on the type of fiber itself. The TPU/pineapple fiber absorbed large amount of both oil compared to others.

REFERENCES

[1] G. Nilza, G. Justix-Smith, J. Vigo and E. Vernon, "Potential of Jamaican banana, coconut coir and baggase fibres as composites materials," *Materials Characterizations*, vol. 59, no. 9, pp 1273-1278, 2008.

[2] N.A. Ahad, N.F.H.M. Radzi, N.S. Sadli and J.S. Tan, "Comparing various type of natural fibers as filler in TPU," *MATEC Web of Conference*, vol. 97, pp 1-7, 2017.

[3] H. Essabir, M.O. Bensalah, D. Rodrique, R. Bouhfid and A. Qaiss, "Biocomposites based on Argan nut shell ans polymer matrix," *Carbohydrate Polymer*, vol. 143, pp 70-83, 2016.

[4] Z.H.T. Faisal. F., Amir, H. Salmah and I. Tahir, "The effect of acetic acid on properties of coconut shell filled low density polyethylene composites," *Indo. J. Chem.*, vol 10, no. 3, pp 334- 340, 2010.

[5] L. Marko, R. Maja, D. Vilma and S. Franc, "Populus seed fibers as natural source for production of oil absorbents," *Journal of Environmental Management*, vol. 114, pp 158-167, 2013.

Pressure history of syngas/air premixed flames propagating in a closed combustion chamber

Manh-Vu Tran[1,*], Gianfranco Scribano[2], Jeong Park[3]

[1)] School of Engineering, Monash University Malaysia, 47500 Bandar Sunway, Selangor Darul Ehsan, Malaysia
[2)] Faculty of Engineering, University of Nottingham Malaysia Campus,
43500 Semenyih, Selangor Darul Ehsan, Malaysia
[3)] Department of Mechanical Engineering, Pukyong National University, Busan, South Korea

[*]Corresponding e-mail: manhvu.tran@monash.edu

Keywords: Deflagration index; maximum peak of pressure; syngas/air

ABSTRACT – In the present study, explosion characteristics of syngas/air flames are investigated in order to evaluate the hazard of the combustion. Results show that maximum peak of pressures, P_{max}, occur at equivalence ratio (ϕ) of 1.2. While explosion times, t_c, are shortest at $\phi = 1.6$. With increasing the H_2 concentration in the fuel blends, the explosion times are shortened, thereby increasing maximum rate of pressure rises, $(dP/dt)_{max}$, and deflagration indexes, K_G. Explosion parameters increase significantly with the increase of initial pressure in the chamber.

1. INTRODUCTION

Explosion of a fuel/air combustible mixture in a closed system is a serious issue because the system might be damaged if there is no proper venting or explosion suppressing device [1]. It is also important in terms of providing a safety recommendation for production, storage, transportation, and usage of fuels.

For an explosion process with the variation of pressure to time in a closed chamber, some important explosion severity parameters could be determined such as maximum explosion pressure (P_{max}), explosion time (t_c), maximum rate of pressure rise $(dP/dt)_{max}$, and deflagration index (K_G) of a combustion [2]. The objective of this study is to determine these important explosion characteristics of syngas/air premixed flames.

2. EXPERIMENT

2.1 Experimental apparatus and methodology

The experiments were conducted in a stainless steel, cylindrical constant volume chamber with a volume of 6.91 L, as shown in Fig. 1. The reactant mixtures in the closed chamber were prepared by supplying individual component gases (H_2, CO, and air) at corresponding partial pressures until reaching a desired initial pressure, P_u. A waiting time of 15 min is necessary to ensure complete mixing and quiescent conditions. The premixed mixtures were ignited at the center of the chamber by a small energy spark ignition. Once the spark was ignited, a flame kernel was formed at the center of the chamber, started propagating outward spherically, and quenched when it touched the walls of the chamber. A time evolution of pressure in the chamber during combustion was recorded at a sample-rate of 100 kHz. The *P–t* data

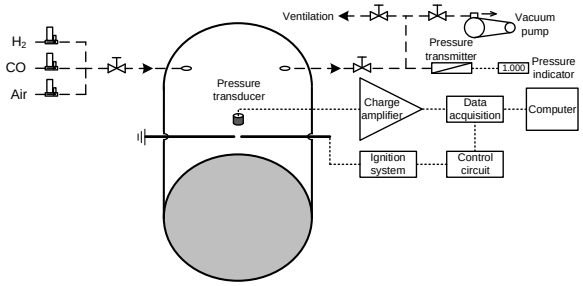

Figure 1 Schematic of experimental setup.

were collected by a water-cooled piezo-electric pressure transducer (Kistler 6061B), connected with a charge amplifier (Kistler 5011B). Then the pressure histories were transferred to computer by a data acquisition (NI 9215A) for later analysis.

2.2 Explosion parameters

The maximum explosion pressure, P_{max}, is defined as the highest pressure reached during the explosion in a closed chamber at a given fuel concentration, and the explosion time, t_c, is the time interval between ignition and the moment when the maximum explosion pressure is attained. The maximum rate of pressure rise, $(dP/dt)_{max}$, is defined as the highest value of pressure rise rate observed at a given fuel concentration, under specific initial temperature and pressure conditions. Because $(dP/dt)_{max}$ depends on the size of the chamber, it is often normalized with respect to the volume of the chamber, V, according to the cubic-root law to define an explosion severity factor so-called deflagration index, $K_G = (dP/dt)_{max} V^{1/3}$.

3. RESULTS AND DISCUSSION

3.1 Effects of H_2/CO concentrations

Figure 2 shows that P_{max} was largest at $\phi = 1.2$ because an adiabatic flame temperature, T_{ad}, of the syngas/air flames is highest at that equivalence ratio, while t_c was shortest at $\phi = 1.6$ due to the combination of the two effects, the T_{ad} and the flame propagating velocity, S_L, which is maximum at $\phi = 2.0$. At a given equivalence ratio, P_{max} and t_c respectively increased and decreased with the increase content of H_2 component in the syngas mixtures. Figure 3 shows that $(dP/dt)_{max}$ and K_G were significantly increased with the enrichment of

the H_2 concentration in the syngas mixtures because of the shortening of the explosion time. This indicates that explosion of the syngas/air premixed flame with high percentage of H_2 is more severe than that of the mixture with high CO concentration. The maximum K_G of all flames occurred at $\phi = 1.6$ corresponding to the shortest t_c happening at the same equivalence ratio.

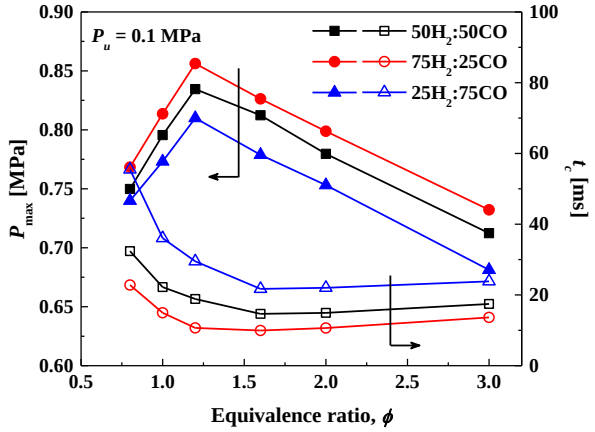

Figure 2 P_{max} and t_c versus ϕ of various syngas/air flames at $P_u = 0.1$ MPa.

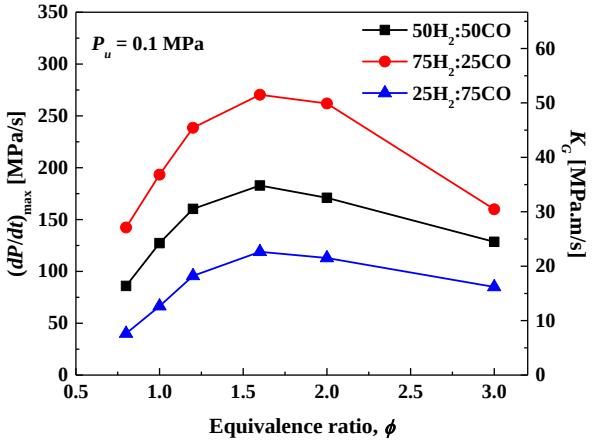

Figure 3 $(dP/dt)_{max}$ and K_G versus ϕ of various syngas/air flames at $P_u = 0.1$ MPa.

3.2 *Effects of initial pressures*

As shown in Fig. 4, P_{max}/P_u of various syngas/air mixtures were increased with the increase of P_u because the T_{ad} is proportional to the P_u in the chamber. In addition, at higher P_u, the flame tends to be turbulent more easily because of the promotion of flame front instability with increasing the P_u [3,4]. The flame front instability causes an increase in the S_L and a shortening in the t_c.

Figure 5 shows that $(dP/dt)_{max}$ and K_G were significantly increased with the increase of the P_u of mixtures. With the increase of the P_u, the flame front becomes more unstable because of the promotion of hydrodynamic instability due to the significant decrease of the flame thickness, thus the flame front is easily developed into a turbulent situation thereby increasing the flame front area [3,4], resulting in a faster flame propagation velocity and a higher rate of pressure rise, corresponding to a higher deflagration index.

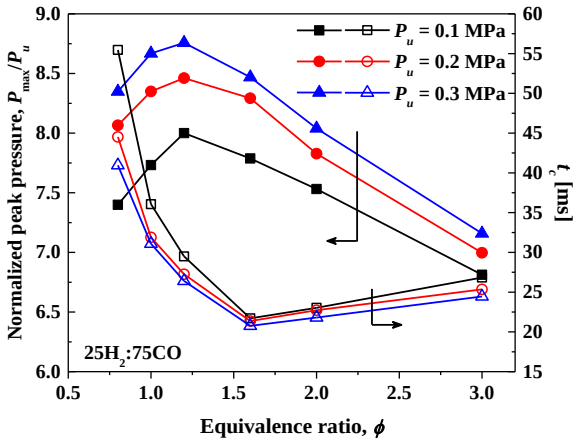

Figure 4 P_{max}/P_u and t_c of the $25H_2$:75CO syngas/air flames at different initial pressures.

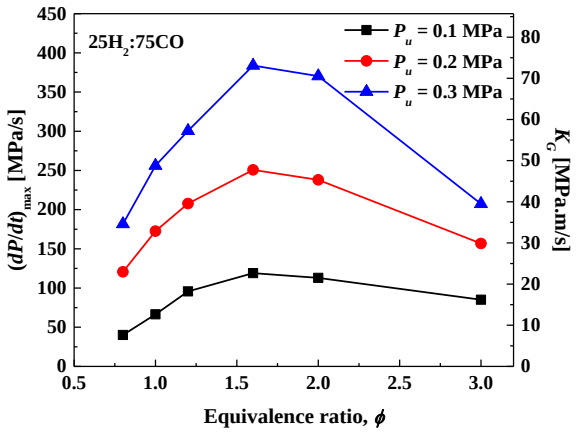

Figure 5 $(dP/dt)_{max}$ and K_G of the $25H_2$:75CO syngas/air flames at different initial pressures.

4. CONCLUDING REMARKS

a) P_{max} occurred at $\phi = 1.2$, t_c was shortest at $\phi = 1.6$.
b) $(dP/dt)_{max}$ and K_G increased/decreased with increasing H_2/CO content in the fuel mixture.
c) P_{max}/P_u, $(dP/dt)_{max}$, and K_G increased along with the initial pressure.

REFERENCES

[1] S. Kundu, J. Zanganeh and B. Moghtaderi, "A review on understanding explosions from methane–air mixture," *J. Loss Prev. Process Ind.*, vol. 40, pp. 507–523, 2016.

[2] C. Movileanu, V. Gosa and D. Razus, "Explosion of gaseous ethylene–air mixtures in closed cylindrical vessels with central ignition," *J. Hazard. Mater.*, vol. 235–236, pp. 108–115, 2012.

[3] T.M. Vu, J. Park, O.B. Kwon and J.S. Kim, "Effects of hydrocarbon addition on cellular instabilities in expanding syngas–air spherical premixed flames," *Int. J. Hydrogen Energy*, vol. 34, pp. 6961–6969, 2009.

[4] T.M. Vu, J. Park, O.B. Kwon, D.S. Bae, J.H. Yun and S.I. Keel, "Effects of diluents on cellular instabilities in outwardly propagating spherical syngas–air premixed flames," *Int. J. Hydrogen Energy*, vol. 35, pp. 3868–3880, 2010.

The rate of moisture absorption and dissipation of plastic materials used in tunable filter microcircuit

P.J. Lee[1,2,*], A.Y. Bani Hashim[1]

[1)] Faculty of Manufacturing Engineering, Universiti Teknikal Malaysia Melaka, Hang Tuah Jaya, 76100 Durian Tunggal, Melaka, Malaysia
[2)] Keysight Technologies, Bayan Lepas Free Industrial Zone, 11900 Penang, Malaysia

[*]Corresponding e-mail: pjiuan@yahoo.com

Keywords: Plastic; moisture absorption; moisture dissipation

ABSTRACT – Tunable filter microcircuit is designed and manufactured as a bandpass filter to filter an unknown incoming signal. It is an assembly combination of various components, such as crystal spheres, crystal rod holder, semi-rings, springs, housing, magnet. The crystal rod holder is made of plastic materials. This work studies the rate of the moisture absorption and dissipation of four different type of plastic materials namely W, X, Y, and Z. The results showed that the rate of moisture absorption and dissipation has a natural logarithmic trend where all materials exhibit a trend of increasing rate over time.

1. INTRODUCTION

Tunable filter microcircuit (TFM) is designed and manufactured as a bandpass filter to filter an unknown incoming signal. TFM is an assembly of various components, such as crystal spheres, crystal rod holder (CRH), semi-rings, springs, housing, magnet. CRH is made of plastic materials. The injection molding process produces the CRH.

The CRH would distort and is no longer at the optimal position within the TFM unit due to the nature of the plastic materials that absorb moisture and deformed over time.

It is hard to determine if the CRH is in an acceptable condition or otherwise by visual inspection or dimension measurement. The defect occurs after exposure to the environment or heat.

This work seeks to find the relationship between the rate of plastic moisture absorption and dissipation over time when exposed to the environment and heat. Also, this work studies the moisture absorption rate for the different grade of plastic materials in the production environment and examines the moisture dissipation rate for a different class of plastic materials in the production environment.

2. LITERATURE REVIEW

Plastic absorbs moisture, moisture inside plastic leads to mechanical deterioration and cause the plastic to swell [1-7]. Garcia et al. [5] mentioned moisture absorption in the plastic increase over time and then to a saturation point. Moisture dissipation can inverse the process, however, might not remain the original plastic properties. One type of moisture absorption test method is the water immersion approach that refers to the ASTM D570-98.

Standard with water absorption (24 hours) method, or the second test which is to load the plastic into humidity chamber or by immersion into liquid solutions. The researchers [4,5,7] use the water immersion methods for moisture absorption analysis. Galloway and Miles [8] and Bhattacharyya et al. [9] use humidity chamber soaking method. Bajpai et al. [10], however, apply the liquid solution immersion method.

3. METHODS

The tool use for new plastic material selection is Radar Chart from Microsoft Excel to compare the shortlisted plastic materials to the current CRH material W. Only four types of plastic grades, inclusive of the current material W were selected for the study due to time and budget constraints.

Samples from the selected plastics materials were prepared using the same mold tool as material W. The experiments were performed by utilizing the available resources, tools, and equipment in the production.

The tools and equipment used were the calibrated Mettler Toledo AG245 balance capable of reading 0.1mg, two units of BlueM ovens with uniform temperatures of 150±5°C and 85±5°C. The samples were exposed to the environment after drying for 15 minutes.

4. RESULTS AND DISCUSSION

Figure 1 shows the measurement taken from the samples received to drying, humidity chamber test, then drying and finally production environment exposure.

The chart has four quadrants where the first quadrant represents the samples with unknown moisture content and underwent moisture dissipation in the oven.

The second quadrant relates to dried samples loaded into humidity chamber for 85°C and 85% relative humidity exposure to determine the saturation point.

The third quadrant refers to the moisture dissipation in the oven after the humidity chamber exposure to study the time taken versus temperature for each plastic. The fourth quadrant refers to moisture absorption exposure at production environment.

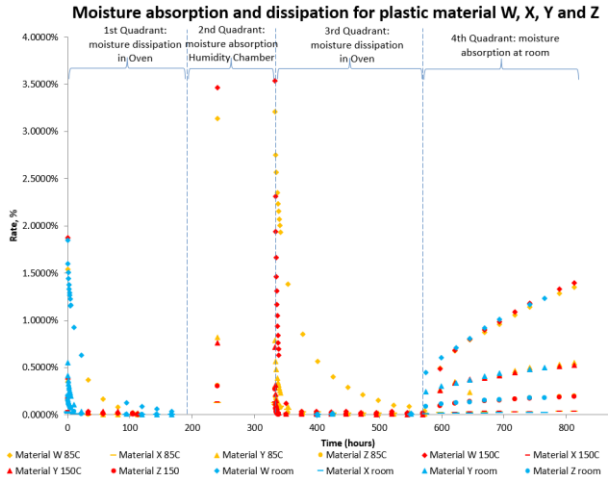

Figure 1 Moisture absorption and dissipation for plastic materials. It is divided into four quadrants where quadrant represents the particular scope of data collection.

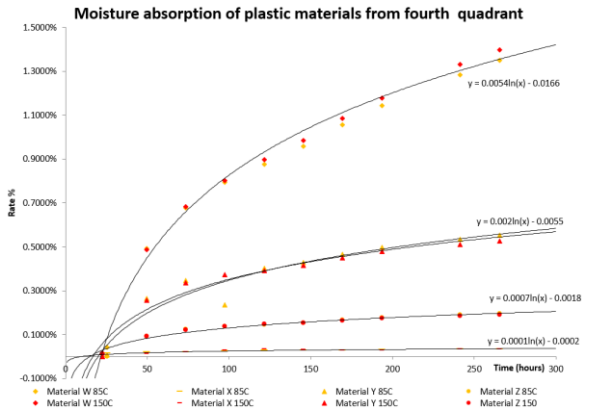

Figure 2 Moisture absorption and dissipation for plastic materials from the fourth quadrant.

Figure 2 depicts the chart with trend lines generated in Microsoft Excel environment. It is to determine the moisture absorption rate for all the four plastic materials over time. The vertical axis represents the dependent variable that is the moisture absorption rate in percentage. The horizontal axis represents the independent variable that is the time. The equations were generated through Microsoft Excel tool. Equation (1) defines the moisture absorption rate as a function of time.

$$\left.\begin{aligned} &\%\ \text{rate W}: r_W(t) = 5.4\times10^{-3}\ln(t) - 1.7\times10^{-3} \\ &\%\ \text{rate X}: r_X(t) = 1.0\times10^{-4}\ln(t) - 2.0\times10^{-4} \\ &\%\ \text{rate Y}: r_Y(t) = 2.0\times10^{-3}\ln(t) - 1.5\times10^{-3} \\ &\%\ \text{rate Z}: r_Z(t) = 7.0\times10^{-4}\ln(t) - 1.8\times10^{-3} \end{aligned}\right\} \quad (1)$$

5. CONCLUSIONS

Although the plastic materials were exposed to the extreme humid condition, material W plastic yet to reach saturation. Materials X, Y, and Z exhibit over saturation and dissipate moisture content over time. At worst case, all the four plastics materials can return to dry state after ten days of baking in the oven at 85±5°C. The trendline equations may be used to estimate the moisture absorption rate after certain exposure time frame. Future study can be conducted to validate the application the optimal plastic for product level qualification.

ACKNOWLEDGEMENT

I would like to thank Paul Cassanego for his supports and collaboration in this studies.

REFERENCES

[1] W.D. Jr. Callister, D.G. Rethwisch, *Materials Science and Engineering An Introduction*, 9th ed. New York: John Wiley & Sons; 2014.

[2] B.C. Ray and D. Rathore, "Durability and integrity studies of environmentally conditioned interfaces in fibrous polymeric composites: Critical concepts and comments," *Advances in Colloid and Interface Science*, vol. 209, pp. 68-83, 2014.

[3] J.S. Earl, R.A. Shenoi, "Hygrothermal aging effects on FRP laminate and structural foam materials." *Composites Part A: Applied Science and Manufacturing*, vol 35 pp. 1237-1247, 2014.

[4] X. Jiang., H. Kolstein., F.S.K. Bijlaard, "Moisture diffusion in glass-fiber-reinforced polymer composite bridge under hot/wet environment," *Composites: Part B*, vol 45, pp 407-416, 2013.

[5] E.J.D. Garcia, F.D. Castro, P.P. Gayo, M.F. Ballester, "Effects of sea water environment on glass fiber reinforced plastic materials used for marine civil engineering constructions," *Materials and Design*, vol 66, pp. 46-50, 2015.

[6] S. Sethi, B.C. Ray, "Environmental effects on fibre reinforced polymeric composites: Evolving reasons and remarks on interfacial strength and stability," *Advances in Colloid and Interface Science*, 217, pp. 43-67, 2015.

[7] S.A. Grammatikos, B. Zafari, M.C. Evernden, J.T. Mottram, J.M. Mitchels, "Moisture uptake characteristics of a pultruded fibre reinforced polymer flat sheet subjected to hot/wet aging," *Polymer Degradation and Stability*, 121, pp. 407-419, 2015.

[8] J.E. Galloway, B.M Miles, "Moisture Absorption and Desorption Predictions for Plastic Ball Grid Array Packages." *IEEE Transactions of Components, Packaging and Manufacturing Technology-Part A*. vol 20, pp. 274-279, 1997.

[9] B.K. Bhattacharyya, W.A. Huffman, W.E. Jahsman , B. Natarajan, "Moisture Absorption and Mechanical Performance of Surface Mountable Plastic Packages," in *Electronics Components Conference, IEEE, Proceedings of the 38th*, 9-11 May 1988.

[10] M. Bajpai, S.K. Bajpai, P. Jyotishi., "Water absorption and moisture permeation properties of chitosan/poly(acrylamide-co-itaconic acid) IPC films," *International Journal of Biological Macromolecules*, 84, pp. 1-9, 2016.

Development of ethylene glycol and water mixture MWCNT-OH based nanofluid with high thermal conductivity

A. Abdullah[1], I.S. Mohamad[1,2,*], A.Y. Bani Hashim[3], N. Abdullah[4], S. Zainal Abidin[1], N.A.B. Masripan[1,2]

[1)] Faculty of Mechanical Engineering, Universiti Teknikal Malaysia Melaka,
Hang Tuah Jaya, 76100 Durian Tunggal, Melaka, Malaysia
[2)] Centre for Advanced Research on Energy, Universiti Teknikal Malaysia Melaka,
Hang Tuah Jaya, 76100 Durian Tunggal, Melaka, Malaysia
[3)] Faculty of Manufacturing Engineering, Universiti Teknikal Malaysia Melaka,
Hang Tuah Jaya, 76100 Durian Tunggal, Melaka, Malaysia
[4)] Centre for Foundation Studies, Universiti Pertahanan Nasional Malaysia,
Kem Sungai Besi, 57000, Kuala Lumpur, Malaysia

[*]Corresponding e-mail: imran@utem.edu.my

Keywords: Thermal conductivity; nanofluids

ABSTRACT – The aim of this paper is to develop nanofluids and investigate the thermal conductivity value of MWCNT-OH based nanofluids where the base fluid is the mixture of EG:DI (20:80) at three different temperatures which are 6°C, 25°C and 40°C. The result reveal the inclusion of nanoparticles which have superior thermal conductivity value in the base fluid make a positive enhancement for all concentrations of MWCNT-OH based nanofluids. The enhancement of nanofluids's thermal conductivity is from 0.8121% to 16.96%. In conclusion, thermal conductivity is strongly depends on the temperature of nanofluids, weight percentage of surfactant and the thermal conductivity of nanoparticles.

1. INTRODUCTION

Many researchers have shown interests in the nanofluids fields since the used of nanoparticles can facilitates the enhancement of thermal and electrical properties of the fluids. Hence, they have superior thermal properties as compare to the conventional fluids such as deionized water (DI), ethylene glycol (EG) and oil [1]. However, limitations are discovered when using conventional fluids in the cooling system application due to low boiling point and a high freezing point of DI. Therefore, an antifreeze additive can be applied to overcome this problem. Previous researcher has stated that, the common fluid used as antifreeze additive are EG and methanol [2]. Thus, the mixture of antifreeze additive with DI in the formulation should improve the thermal properties of the fluid with proper concentration. Previous literature stated that, thermal conductivity of H_2O:EG based fluids with 1.0 vol% of SiC gives an enhancement about 33.84% at temperature 20°C [3]. Moreover, the enhancement of thermal conductivity of nanofluids with formulation of 60:40;EG:DI increases from 6.67% up to10.47% [4]. The thermal conductivity enhancement is still under investigation where the mixture between two types of conventional fluids is rarely study by the researcher. Therefore, this work investigates thermal conductivity of EG:DI mixture (20:80) with -OH functionalized multiwalled carbon nanotube (MWCNT-OH) based nanofluids as to fill the research gap.

2. METHODOLOGY

Hydroxyl functionalized Multiwalled Carbon Nanotubes (MWCNT-OH) nanoparticles used in this investigation were purchased from Nanostructures & Amorphous Material, Inc and surfactant polyvinylpyrrolidone (PVP) were purchased from Sigma Adrich Co. Whilst, the appropriate volume of EG and DI (20:80) were mixed together as a base fluid. All these formulations were prepared by two-step method. Firstly, an amount of MWCNT-OH was mixed into the base fluid from range 0.1 wt% to 1.0 wt% with inclusion of 0.1 wt% PVP in a clear sampling glass bottle. Then, the mixture was further homogenized and sonicated at the same time to achieved good dispersion using Wise Tis HG-15D homogenizer at 10000 rpm and Branson 8510DTH Ultrasonic Cleaner at 40 kHz for five minutes. The samples were shelved for 100 hours and the stability of the fluid was monitored by stability test rig (STR) [1]. The stable nanofluids were further test for their thermal conductivity properties by TC-KD2 Pro thermal analyser using of KS1 sensor at three different temperatures which are 6°C, 25°C and 40°C.

3. RESULTS AND DISCUSSION

Figure 1 shows the thermal conductivity of EG:DI based MWCNT-OH nanofluids at several concentrations ranging from 0.1 wt% to 1.0 wt% with 0.1 interval. Closer inspection on this plot, it shows that a significant improvement on the thermal conductivity value in the formulations. The standard thermal conductivity values of base fluid without the addition of nanoparticles for each temperature are 0.4440 W/m.K, 0.4556 W/m.K and 0.4600 W/m.K for temperature 6°C, 25°C and 40°C. The straight line in the figure represents the standard value line of base fluids. Interestingly, the highest thermal conductivity was achieved for 0.9 wt% of MWCNT-OH in the base fluid with value given 0.5380 W/m.K at temperature 40°C, 0.5170 W/m.K at

25°C and 0.4883 W/m.K at 6°C. This was followed by 0.3 wt% of MWCNT-OH with thermal conductivity value given 0.5170 W/m.K, 0.5063 W/m.K and 0.4850 W/m.K for 40°C, 25°C and 6°C. However, maximum concentration of 1.0 wt% results in no major influence on the thermal conductivity values with only 0.4810 W/m.K at 40°C, 0.4593 W/m.K at 25°C and 0.4623 W/m.K at 6°C. To sum up, all the thermal conductivity values of nanofluids is higher than the base fluid for all temperatures. In addition, the thermal conductivity of nanofluids is strongly depends on temperature where the high temperature tend to make the nanoparticles move and collide to each other and create the high energy transfer. However, high temperatures also can form the agglomeration in nanofluids and causes the reduction of thermal conductivity. Besides, previous research revealed that the inclusion of lower weight percentage of surfactant also influenced the increment of thermal conductivity value [5].

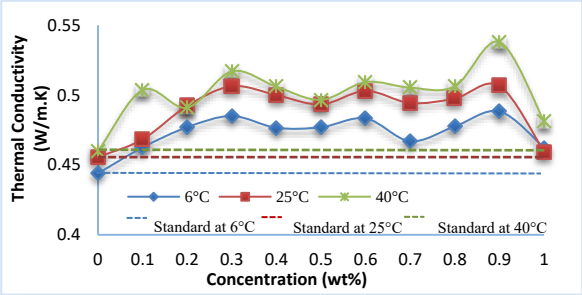

Figure 1 Thermal conductivity of EG:DI based nanofluid.

Table 1 shows the percentage enhancement of thermal conductivity for each concentration of nanofluids. The highest thermal conductivity enhancement occurs at the temperature of 40°C which about 16.96% and 12.39% for 0.9 wt% and 0.3 wt% of MWCNT-OH based nanofluids. Meanwhile, the lowest thermal conductivity enhancement is found out at concentration of 1.0 wt% MWCNT-OH based nanofluids for temperature 25°C which only 0.8121%.

Table 1 Percentage enhancement of thermal conductivity.

Concentration (wt%)	% Enhancement of Thermal Conductivity (W/m.K)		
	6°C	25°C	40°C
0.1	4.167	2.787	9.478
0.2	7.432	8.055	6.739
0.3	9.234	11.13	12.39
0.4	7.342	9.745	10.00
0.5	7.432	8.275	7.956
0.6	8.851	10.40	10.72
0.7	5.180	8.494	9.848
0.8	7.567	9.219	10.06
0.9	9.977	11.19	16.96
1.0	4.122	0.8121	4.565

To conclude, all concentrations of MWCNT-OH based nanofluids shows positive enhancement as the addition of nanoparticles which have superior thermal conductivity value compared to the conventional fluid. Thus, this fact is supported by previous researcher where the thermal conductivity enhanced with the dispersion and suspension of nanomaterials that have higher thermal conductivity into the base fluids [6].

4. CONCLUSION

The addition of nanoparticles in the base fluid mixture of EG as the anti-freezing additive with DI can contribute to the increment of thermal conductivity value. The values were found to be higher than the standard base fluids at all temperatures. The optimum condition with better thermal conductivity enhancement was achieved by 0.9 wt% of MWCNT-OH. Some issues that affected the thermal conductivity results is temperature where high temperature can enhance and lowers the thermal conductivity. The lower weight percentage of surfactant and thermal conductivity of nanoparticles are also another factor that can influence and enhance the thermal conductivity value of nanofluids.

ACKNOWLEDGEMENT

This work was supported by the grants below:
FRGS/2010/FKM/SG-03/1-F0076
FRGS/2/2013/SG02/UTeM/02/1
FRGS/2/2013/ST05/UPNM/03/1

REFERENCES

[1] S. Mohamad, S.B.A. Hamid, W.M. Chin, K.H. Yau and A. Samsuri, “Nanofluid-based nanocarbons: An investigation of thermal conductivity performance,” *Journal of Mechanical Engineering and Technology,* vol. 3, no. 1, pp. 79-87, 2011.

[2] F. Conrad, E. Hill and E. Ballman, “Freezing points of the thermal system ethylene glycol-methanol-water,” *Industrial & EngineeringChemistry,* vol. 32, no. 4, pp. 542-543, 1940.

[3] X. Li and C. Zou, "Thermo-physical properties of water and ethylene glycol mixture based SiC nanofluids: An experimental investigation", *International Journal of Heat and Mass Transfer*, vol. 101, pp. 412-417, 2016.

[4] A. Ijam, R. Saidur, P. Ganesan and A. Moradi Golsheikh, “Stability, thermo-physical properties and electrical conductivity of graphene oxide-deionized water/ethylene glycol based nanofluids,” *International Journal of Heat and Mass Transfer*, vol. 87, pp. 92-103, 2015.

[5] Z. Mingzheng, X. Guodong, L. Jian, C. Lei and Z. Lijun, “Analysis of factors influencing thermal conductivity and viscosity in different kinds of surfactant solutions,” *Experimental Thermal and Fluid Science,* vol. 36, pp. 22-29, 2012.

[6] N. Singh, G. Chand and S. Kanagaraj, “Investigation of thermal conductivity and viscosity of carbon nanotube-ethylene glycol nanofluid,” *Heat Transfer Engineering*, vol. 33, no. 9, pp. 821-825, 2012.

Optimization parameter for high thermal conductivity and heat transfer using ethylene glycol and water mixture MWCNT-OH based nanofluids

A. Abdullah[1], I.S. Mohamad[1,2,*], A.Y. Bani Hashim[3], N. Abdullah[4], S. Zainal Abidin[1]

[1)] Faculty of Mechanical Engineering, Universiti Teknikal Malaysia Melaka, Hang Tuah Jaya, 76100 Durian Tunggal, Melaka, Malaysia
[2)] Centre for Advanced Research on Energy, Universiti Teknikal Malaysia Melaka, Hang Tuah Jaya, 76100 Durian Tunggal, Melaka, Malaysia
[3)] Faculty of Manufacturing Engineering, Universiti Teknikal Malaysia Melaka, Hang Tuah Jaya, 76100 Durian Tunggal, Melaka, Malaysia
[4)] Centre for Foundation Studies, Universiti Pertahanan Nasional Malaysia, Kem Sungai Besi, 57000, Kuala Lumpur, Malaysia

[*]Corresponding e-mail: imran@utem.edu.my

Keywords: Thermal conductivity; heat transfer; nanofluids

ABSTRACT – The objective of this paper is to measure and analyze the thermal conductivity and heat transfer of ethylene glycol and deionized water mixture of MWCNT-OH based nanofluids (EG:DI;10:90) at three different temperatures (6°C, 25°C and 40°C). Two-step method is used in the preparation of nanofluids through mixing of the MWCNT-OH, base fluids and polyvinylpyrrolidone by dispersion process. The result shows the increment of thermal conductivity from 0.7590% to 13.42% and the enhancement of heat transfer is about 250%. Several issues are discovered to have affected the thermo-physical tests which are nanoparticles size, temperature, dispersion process and sedimentation of particles.

1. INTRODUCTION

Nanofluids is the suspension of nanoparticles of either metallic or non-metallic in the base fluid (ethylene glycol, *EG,* water, H_2O or oil) [1]. It plays an important role in addressing the issue of cooling system applications as it can enhance the thermal performance of fluids. This is due to the nanoparticle characteristics which have a high thermal conductivity, electrical conductivity, and heat transfer. However, H_2O base fluid has lower freezing point that which might lead to limitation in some cooling applications. Therefore, the mixture of H_2O and EG as heat transfer fluid is an alternative way to overcome this problem due to low freezing point of EG respectively. Hence, a number of studies have conducted the thermal properties of EG and H_2O mixture based nanofluids experiment and stated that the increment of thermal conductivity is about 9.8% to 17.89% for mixture of EG and H_2O at 50:50 wt% and 6.67% to 10.47% enhancement for 60:40 wt% (EG:DI) [2,3]. Whilst, for the heat transfer investigation which was performed at 50°C the mixture base of H_2O to EG (60:40) has 14.6% enhancement on 0.6% volume concentration of Al_2O_3 [4]. Wherefore, to fill the research gap, this research focuses on the thermal conductivity and heat transfer of -OH functionalized multiwalled carbon nanotube (MWCNT-OH) based nanofluids in the EG:DI mixture (10:90).

2. METHODOLOGY

Two-step method was use in the synthetization of nanofluids. The formulation of the nanofluid comprises of the MWCNT-OH developed by Nanostructures & Amorphous Material, Inc with a weight percentage, *wt%* range of 0.1 wt% till 1.0 wt% with an increment 0.1 wt% respectively. In order to stabilize the suspended particles of MWCNT-OH in the nanofluid, polyvinylpyrrolidone, *PVP* developed by Sigma Aldrich Co. with a 0.1 wt% is used. It is noted that the base fluid used is a mixture of EG and DI with a ratio of 10% and 90% respectively (EG:DI;10:90). This composition of CNT, base fluid and stabilizer undergoes dispersion process for five minutes through homogenization (Wise Tis HG-15D homogenizer) at 10000 rpm and ultrasonication (Branson 8510DTH Ultrasonic Cleaner) at 40 kHz. The stability of the nanofluids is determined through a stability test rig, *STR* [1]. In order to determine the thermo-physical properties of nanofluids, refrigerated water bath was used to conduct the thermo-physical test at three different temperatures (6°C, 25°C, and 40°C). TC-KD2 Pro was used in the thermal conductivity test where KS-1 sensor inserted to the nanofluids sample and reading was taken in one minute for three times. The accuracy value of this sensor is ±0.01 W/m.K. Heat transfer test is then conducted using copper coil submerged in the water bath at the designated temperature where the nanofluids is flowed through the coil by water pump and measured with Pico Data Logger. The temperature accuracy of Pico Data Logger is sum of ±0.2% of reading and ±0.5°C.

3. RESULTS AND DISCUSSION

3.1 Thermal conductivity

Figure 1 shows the thermal conductivity of nanofluids with the formulated concentrations at three different temperatures. It is observed that the thermal conductivity of the nanofluids is higher than the base fluid (0 wt%) for all temperatures level and the straight line is represented the standard values for the base fluid. The results in the Figure 1 indicate the higher thermal

conductivity for all temperatures occurred on 0.7 wt%, 0.8 wt% and 0.9 wt%. At 40°C, 0.9 wt% of MWCNT-OH has the highest thermal conductivity compared to the others sample where the value is 0.6340 W/m.K and the enhancement is approximately 13.42%. Whilst, at 25°C for 0.1 wt% of MWCNT-OH has the lowest thermal conductivity value which is 0.5310 W/m.K and the thermal conductivity enhancement is only 0.7590%.

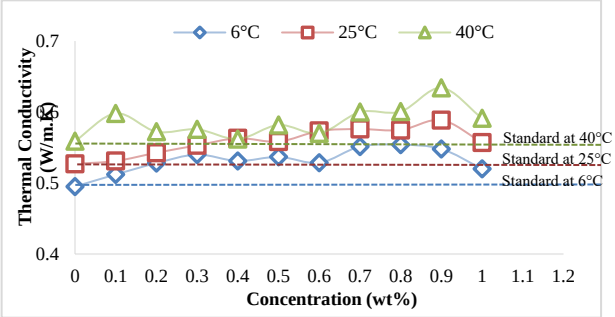

Figure 1 Thermal conductivity of EG:DI based nanofluid.

3.2 Heat transfer

Figure 2 presents the temperature differences for MWCNT-OH concentration at 0.7 wt%, 0.8 wt% and 0.9 wt% at 6°C, 25°C and 40°C. These concentrations were selected for the heat transfer test due to their enhancement in the thermal conductivity test results in the highest among the others concentration. Closer inspection of the figure shows at 40°C for 0.7 wt% has the highest temperature differences and the heat transfer enhancement is about 250%. 0.8 wt% of MWCNT-OH results in a lower temperature difference for 6°C and 25°C as compared to the standard.

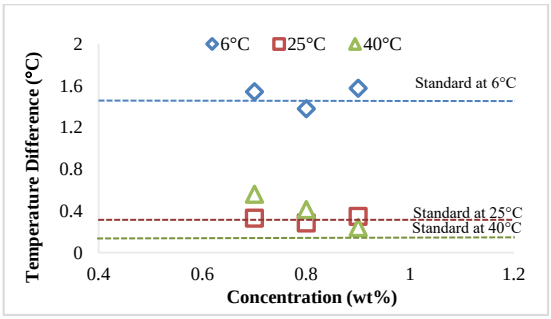

Figure 2 Temperature differences at 6°C, 25°C and 40°C.

Thermal conductivity and heat transfer property are related to each other where higher thermal conductivity can give the better result in heat transfer test. These enhancements can be due to the characteristic of MWCNT-OH having a small size and large surface area where the outer diameter is about 10 nm to 30 nm and the inner diameter is 5 nm to 10 nm and resulting in a higher thermal conductivity due to a larger heat absorption and capacity [5]. Besides, thermo-physical properties strongly depend on the temperature where the highest enhancement occurs at 40°C for both experiment as the high temperature can make the nanoparticles is more active which enables more energy transfer. Meanwhile, the crucial factor is the dispersion process where the vibration from the ultrasonic and homogenizer can make the nanoparticles dispersed well in the fluids and achieved the stability [1]. However, the sedimentation form at a certain period can decrease the thermo-physical properties as nanofluids have more than one-month lifetime of stability. This fact is justified on some concentrations of the nanofluids which exhibits no enhancements in thermo-physical properties.

4. CONCLUSION

In conclusion of MWCNT-OH nanoparticles into the base fluid (EG:DI;10:90) can enhance the thermo-physical properties is proved where the thermal conductivity enhancement is about 0.7590% at 0.1 wt% (25°C) and 13.42% at 0.9 wt% (40°C). Whilst, the heat transfer enhancement is about 250% at 0.7 wt% for 40°C. Factor that influenced these thermo-physical results are the small size and large surface area of MWCNT-OH, high temperatures that enable the nanoparticles become more active and transfer more energy, the dispersion process and as well as the sedimentation form in nanofluids.

ACKNOWLEDGEMENT

This study was supported by grants:
FRGS/2010/FKM/SG-03/1-F0076
FRGS/2/2013/SG02/UTeM/02/1
FRGS/2/2013/ST05/UPNM/03/1

REFERENCES

[1] A. Abdullah, I.S. Mohamad, A.Y. Bani Hashim, N. Abdullah and S. Zainal Abidin, “Effect duration time of homogenization and sonication on stability of MWCNT-OH in ethylene glycol and deionized water,” in *Proceedings of Mechanical Engineering Research Day*, 2016, pp.171-172.

[2] L.S. Sundar, M.H. Farooky, S.N. Sarada and M.K. Singh, “Experimental thermal conductivity of ethylene glycol and water mixture based low volume concentration of Al_2O_3 and CuO nanofluids,” *International Communication in Heat and Mass Transfer,* vol. 41, pp.41-46, 2013.

[3] AIjam, R. Saidur, P. Ganesan and A. Moradi Golsheikh, “Stability, thermo-physical properties and electrical conductivity of graphene oxide-deionized water/ethylene glycol based nanofluids,” *International Journal of Heat and Mass Transfer*, vol. 87, pp.92-103, 2015.

[4] N. Usri, W. Azmi, R. Mamat, K. Hamid and G. Najafi, "Heat transfer augmentation of Al_2O_3 nanofluid in 60:40 water to ehylene glycol mixture,” *Energy Procedia*, vol. 79, pp. 403-408, 2015.

[5] I.S. Mohamad, S.T. Chitrambalam, S.B.A. Hamid, W.M. Chin, K.H. Yau and I. Febrian,“Comparison study on the heat transfer behavior on aqueous suspensions of rod shaped carbon nanotubes,” *Advanced Materials Research*, vol. 667, pp. 35-42, 2013.

Thermal conductivity of carbon nanofiber in EG-DI based nanofluids

S. Zainal Abidin[1], I.S. Mohamad[1,2,*], A.Y. Bani Hashim[3], N. Abdullah[4], A. Abdullah[1]

[1)] Faculty of Mechanical Engineering, Universiti Teknikal Malaysia Melaka,
Hang Tuah Jaya, 76100 Durian Tunggal, Melaka, Malaysia
[2)] Centre for Advanced Research on Energy, Universiti Teknikal Malaysia Melaka,
Hang Tuah Jaya, 76100 Durian Tunggal, Melaka, Malaysia
[3)] Faculty of Manufacturing Engineering, Universiti Teknikal Malaysia Melaka,
Hang Tuah Jaya, 76100 Durian Tunggal, Melaka, Malaysia
[4)] Department of Chemistry, Centre for Foundation Studies, Universiti Pertahanan Nasional Malaysia,
Kem Sungai Besi, 57000, Kuala Lumpur

*Corresponding e-mail: imran@utem.edu.my

Keywords: Carbon nanofiber; thermal conductivity; nanofluids

ABSTRACT – This paper was aimed at formulating a stable nanofluid from CNF HHT24 in a base fluid consisting of deionized water (DI) and ethylene glycol (EG) with the presence of polyvinylpyrrolidone (PVP) as dispersing agent. The experiment was conducted by setting the variable weight percentage of CNF from 0.1wt% to 1.0wt%, with the base fluid ratio being 70:30 (DI:EG) weight percent. Then, the thermal conductivity was investigated at three different temperatures which are at 6ºC, 25ºC and 40ºC. The highest thermal conductivity was gained at 1.0wt% at temperature 40°C with thermal conductivity value of 0.499 W/m.K. Meanwhile, the highest percentage enhancement in thermal conductivity were obtained by 1.0wt% at 40ºC with 6.62%. Overall, nanofluids proved to have a greater potential to be commercialized as conventional heat transfer fluids due to its good thermal properties.

1. INTRODUCTION

Highly thermally conductive particles such as carbon nanotubes, metal and metal oxides which possess high thermal conductivity have concerned researchers to investigate the performance of existing heat transfer system by adding these materials into a heat transfer fluid to improve the thermal conductivity [1]. Scientists at Argonne National Laboratory was the first one who invented nanofluids by the dilution of liquid particle mixtures which improves the thermal conductivity values of about 20-150% higher than the conventional heat transfer fluids [2]. Numerous studies had been reported in literature regarding the enhancement of thermal conductivity of nanofluids which was prepared by mixing the nanocarbon with conventional base fluids such as water and ethylene glycol. However, only a few studies regarding the addition of carbon nanofiber into a base fluid have been reported. The amazing thermal capability of nanofluid have make these fluids potentially to be used as superior medium for a heat transfer media. Thus, the focus of this study is to formulate a stable nanofluids produced from the mixture of carbon nanofiber (CNF HHT24), base fluid (DI and EG) and dispersing agent.

Then, the thermal conductivity of formulated nanofluid with varying volume concentrations ranging from 0.1wt% to 1.0wt% are studied.

2. METHODOLOGY

2.1 Nanofluids preparation

The nanofiber used in this research were Pyrograf III Carbon Nanofiber HHT24. The polyvinylpyrrolidone (PVP) from Sigma-Aldrich Co. was chosen as a dispersing agent. The nanofluids were synthesized with varying volume concentrations ranging from 0.1wt% to 1.0wt% with the base fluid ratio of 70:30 (DI:EG) weight percent. These mixtures are then homogenized using the mechanical homogenizer for five minutes by using a Digital Homogenizer LHG-15 at 10000 rpm rotational speed. The mixture then was ensured to be dispersed uniformly using ultrasonic at 25ºC for 5 minutes at 37 kHz frequency. The nanofluid dispersion and stability were then observed by using Stability Test Rig (STR) as to make sure the nanofluid were well dispersed.

2.2 Thermal conductivity measurement

All the samples which had been stabilised then were tested for their thermal conductivity. A KD2-Pro Thermal Properties Analyser (Decagon Devices, Inc.) was used to measure the thermal conductivity at three different temperatures of 6°C, 25°C and 40°C. These three temperature was selected to study the temperature effect to the thermal conductivity of nanofluids. A single-needle KS-1 sensor, with a length of 60 mm and a diameter of 1.3 mm, was used to measure the thermal conductivity.

3. RESULTS AND DISCUSSION

The thermal conductivity of nanofluid for volume concentration ranging from 0.1wt% to 1.0wt% with respect to temperature is shown in Figure 1. The results also include the standard thermal conductivity data for mixture of 70:30 (DI and EG). The graph from Figure 1 shows that most of the nanofluid samples exhibited an increasing thermal conductivity higher than the standard suspension.

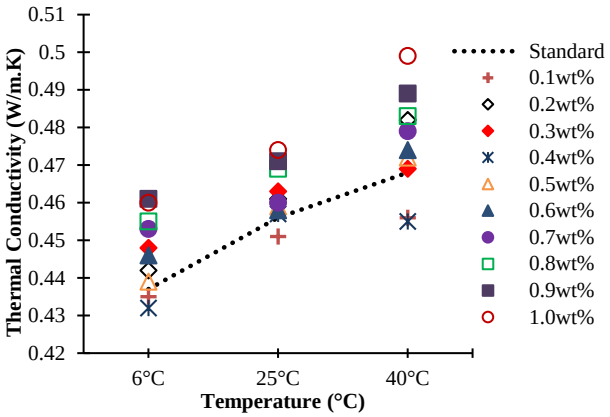

Figure 1 Thermal conductivity of nanofluids in various concentration.

The results show variability for all the temperatures, but it could be seen that the rise in thermal conductivity varied with an increment in nanofluid concentration. The highest thermal conductivity was obtained at temperature 40°C for 1.0wt% with thermal conductivity value of 0.499 W/m.K. However, there were two samples with conductivities that were exceptionally lower than the standard, and these were the 0.1wt% and 0.4wt% samples. The possible reason was because ethylene glycol had a lower thermal conductivity compared to deionized water. Thus, when these two fluids were mixed together, it led to a decrease in thermal conductivity. The enhancement analysis was done to observe the trend, which was compared to the standard fluid. The enhancement percentages of the nanofluids are shown in Table 1.

Table 1 Enhancement percentage of nanofluids.

Volume Concentration (wt%)	**Percentage of Enhancement (%) at Temperature (°C)**		
	6	**25**	**40**
0.1	-0.45	-1.09	-2.56
0.2	1.14	1.10	2.99
0.3	2.52	1.53	0.21
0.4	-1.14	0.22	-2.78
0.5	0.46	0.65	0.85
0.6	2.06	0.44	1.28
0.7	3.66	0.88	2.35
0.8	4.12	2.85	3.20
0.9	5.49	3.29	4.48
1.0	5.26	3.94	6.62

At 6°C, nanofluid sample with 0.9wt% had the highest enhancement in thermal conductivity with 5.49% percent enhancement. Meanwhile, at 25°C and 40°C, the highest enhancement in thermal conductivity was represented by 1.0wt% with 3.94% and 6.62% respectively. The negative value indicated that there was no improvement in the thermal conductivity, which means that the thermal conductivity was lower than the standard suspension. It can be clearly seen from Table 1 that there was no enhancement for the 0.1wt% and 0.4wt% samples. Various reviews and studies covering factor which effect the thermal conductivity of nanofluids have been reported. Gao et al. has revealed the increase in cluster size of nanoparticles has significant impact on the enhancement of thermal conductivity [3]. Some previous studies also reported a linear relation between increasing of thermal conductivity with increasing of particle volume fraction. However, there are also some studies reported a non-linear behavior in thermal conductivity. The possible reason was due to the increase in nanofluids concentration which cause the viscosity of base fluid to increase and consequently cause a reduction in thermal conductivity of nanofluids [4]. The viscosity of the base fluid affects the Brownian motion of nanoparticles and the thermal conductivity of the nanofluid [5-6].

4. CONCLUSION

These findings suggest that the addition of CNF HHT24 nanocarbon into a mixture of ethylene glycol and deionized water as base fluid has proved to exhibit enhancements in their thermal conductivity value. The highest thermal conductivity was gained at 1.0wt% volume concentration at 40°C with thermal conductivity value of 0.499 W/m.K. Overall, nanofluids proved to have a wide prospect to be commercialized as conventional heat transfer fluids due to its good thermal capability.

ACKNOWLEDGEMENT

Authors would like to thank Universiti Teknikal Malaysia Melaka (UTeM) and the Ministry of Higher Education (MOHE) for supporting this research under the grants FRGS/2/2013/SG02/FKP/02/2/F00176.

REFERENCES

[1] M.A. Sabiha, R.M. Mostafizur, R. Saidur and S. Mekhilef, "Experimental investigation on thermo physical properties of single walled carbon nanotube nanofluids," *Int. J. Heat Mass Transfer,* vol. 93, pp. 862-871, 2016.

[2] A. Nasiri, M. Shariaty-Niasar, A. Rashidi and R. Khodafarin, "Effect of CNT structures on thermal conductivity and stability of nanofluid," *Int. J. Heat Mass Transfer,* vol. 55, no. 5, pp. 1529-1535, 2012.

[3] J. Gao, R. Zheng, H. Ohtani, D. Zhu and G. Chen, "Experimental investigation of heat conduction mechanisms in nanofluids: clue on clustering," *Nano Lett.,* vol. 9, no. 12, pp. 4128-4132, 2009.

[4] T.H. Tsai, L.S. Kuo, P.H. Chen and C.T. Yang, "Effect of viscosity of base fluid on thermal conductivity of nanofluids." *Appl. Phys. Lett,* vol. 93, no. 23, pp. 1-3, 2008.

[5] S.N. Syed Idrus, N.S. Zaini, I.S. Mohamad, N. Abdullah and M. H. Mohd Hussin, "Comparison of thermal conductivity for HHT-24 CNF based nanofluid using deionized water and ethylene glycol," *Jurnal Teknologi,* vol. 77, no. 21, pp. 85-89, 2015.

[6] I.S. Mohamad, S.B.A. Hamid, W.M. Chin, K.H. Yau and A. Samsuri, "Nanofluid-based nanocarbons: an investigation of thermal conductivity performance," *Journal of Mechanical Engineering and Technology,* vol. 3, no. 1, pp 79-87, 2011.

Photovoltaic thermal combination of water and air based using active system

F.A. Sachit[1,3], N. Tamaldin[1,2,*], M.A.M. Rosli[1,2]

[2)] Faculty of Mechanical Engineering, Universiti Teknikal Malaysia Melaka,
Hang Tuah Jaya, 76100 Durian Tunggal, Melaka, Malaysia
[2)] Centre for Advanced Research on Energy, Universiti Teknikal Malaysia Melaka,
Hang Tuah Jaya, 76100 Durian Tunggal, Melaka, Malaysia
[3)] Ministry of Electricity, Baghdad Safi Al-Den Al Hilly St, Republic of Iraq

[*]Corresponding e-mail: noreffendy@utem.edu.my

Keywords: Photovoltaic thermal; electric; hot water

ABSTRACT – Hybrid photovoltaic/thermal collectors are devices that simultaneously converts solar energy into electricity and heat. A significant amount of research on PV/T collectors has been carried out over the last 25 years. The review covers experimental work and qualitative evaluation of thermal/electrical output for the water and air based system. This article gives a review about photovoltaic/thermal system and their classification.

1. INTRODUCTION

The recent development programs and research focus on the use of sun energy for solar distillation, hot water or hot air generation. Sun energy system can be used for cooling and heating the space, solar thermal electricity production, building integrating photovoltaic systems and solar refrigeration [1]. In general, solar systems are divided into photovoltaic technology and solar thermal systems. Photovoltaic systems are used to convert the solar radiations into electricity while solar thermal systems can be used for air or water heating applications. Normally, solar thermal systems and photovoltaic technologies are standalone systems. The small photovoltaic system efficiency and space limitation on building's roof for the installation of separate system (PV technologies and thermal systems) have become important factors of combining the thermal systems and photovoltaic technologies in single unit called photovoltaic thermal solar collector system. Therefore, the current research, development and mass production for photovoltaic will minimize their high cost and encourage their application to meet the needs in the thermal solar systems demand. A photovoltaic solar thermal water heater (PVT) is a system that combines the photovoltaic panel and solar thermal collector in one hybrid module. It produces electricity and hot water. The main components of PVT system are the photovoltaic panel, absorber plate (to circulate the working fluid air or water, to cool the PV panel). A proper insulation material should be incorporated to limit the heat losses from system.

1.1 Solar PV/T Systems

When the operating temperature increases, the efficiency of a PV solar cell decreases hence cooling them is necessary. For this, people extract produced heat from panel and use that heat energy for other applications like water heating, this combined system known as Solar PV/Thermal (PV/T) system. For cooling, a fluid is circulated on rear surface of solar PV panel. solar thermal systems incorporate photovoltaic (PV) technologies. By replacing or augmenting absorber plates with photovoltaic cells, it may be possible to increase total solar conversion efficiency. The solar radiation that are absorbed from the sun are converted to electricity partially by the PV cells and partly of the excess heat generated in them is transferred to the heat exchanger in thermal contact with the PV cells while the rest is lost to the ambient. Heat can be extracted from panel using fluid flow method, but heat extraction is not up to the mark in such systems. Thus, the advantages of the PV/T system are:
1) System addresses the majority of building's energy requirement, which is both heat and electricity.
2) Electrical efficiency of panel increased due to reduction in operating temperature of panel.

2. TYPES OF PV/T SYSTEMS

The thermal demand can be enclosed by choosing the appropriate PV/T system. Depending upon the type of module as well its design, type of heat-removal fluid (water/glycol or air), concentration of the incoming radiation, there are various forms of PV/T system [2]. The schematic of a PV/T solar system is shown in Figure 1.

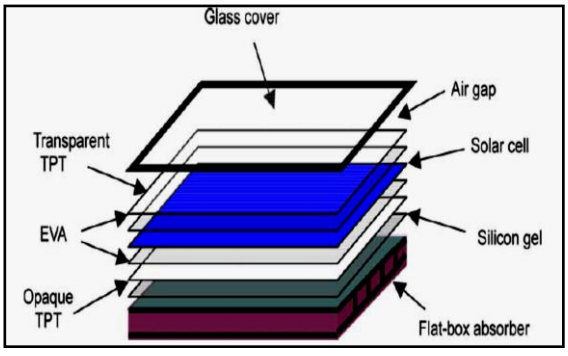

Figure 1 Schematic of a PV/T solar system [3].

2.1 Flat plate collector PV/T system

The flat plate PV/T collector has the appearance like a flat plate thermal collector. There is one PV panel which is attached on the top of metallic absorber plate. The PV module, glass covers well as the absorption plate (Heat exchanger plate) are the contents of PV panel inside of the panel. Zondag et al. [4] has elaborated the PV/T collector types. As shown in Fig (2). the collector comprised of sheet and tube(i), channel (ii), free flow (iii) and two-absorber types (iv) PV/T flat plate collector can be classified into liquid PV/T collector, combination of liquid/air PV/T collector and air PV/T collector, depending on the type of working fluid used. The absorber collector plays an important function in the PV/T system. It cools down the PV cell or module, and also collects the thermal energy produced in the form of hot water or hot air. When this process is going on, the efficiency of the PV cell or module increases [5], [6]. For water type, it can be distinguished according to the water flow pattern and different types of PV/T collector systems are shown in Figure 2 [4].

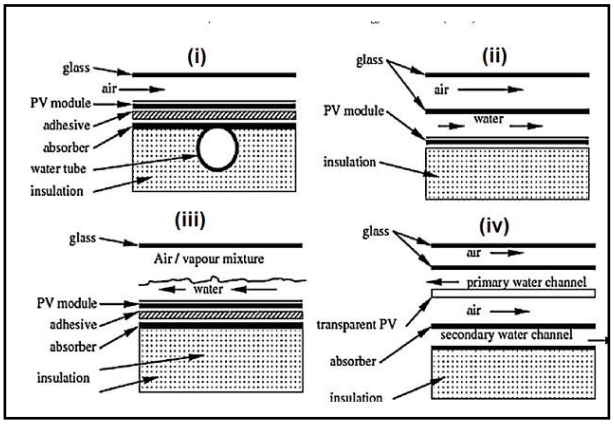

Figure 2 Different types of PV/T collectors [4].

2.2 Combination of liquid/air PV/T collector

The combination of more than one system in a single system is one of the modern techniques and applications in the field of solar energy, especially in the PV/T, which would open horizons and new area will directly add to increasing the amount of the spread of their applications on a greater scale. According to the flow impression of the water or air, Combination of water and/or air type collectors can be distinguished as shown in Figure 3 [6]. In water type PV/T collectors, the main parameters that are necessary to be taken under consideration such as sheet and tube, channel, medium (fluid) flow and the absorber collector types. Tonui and Tripanagnostopoulos [7] performed an experiment to improve PV/T solar collector with heat extraction by natural or forced air circulation. The study contains the possibility of generating electricity and heat energy from commercial PV module adopted as a PVT/AIR solar collector either with forced or natural flow. Another development of combination of water and air type of PV/T collector has been designed by Tonui and Tripanagnostopoulos [8]. They designed the system that utilized both water and air to produced hot water and at the same time produced hot air simultaneously. Assoa et al. has been developed and constructed a two-dimensional mathematical model of bi-fluid PV/T (water and air) collector with a metal absorber collector [9]. They designed a channel shape of a ribbed sheet steel absorber collector. They concluded that the solar collector mass flow rate has influenced on the solar air collector behavior due to some thermal losses exist between the solar air collector and the solar water collector.

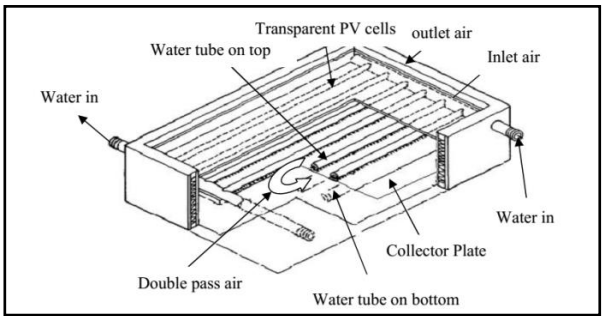

Figure 3 Diagram of PV/T combination flat plate collector [6].

3. CONCLUSION

PV/T systems designed to extract heat from PV modules, heating water or air, aiming to reduce the operating temperature of PV modules and to observe the electrical efficiency at a sufficient level. A comparative study of different PV/T systems is done. Many researchers conclude that the possibility of generating electricity and heat energy from PV/T with either water or air flow. The purpose of PV/T combination system to produces three applications in one system. PV/T combination system that produces electricity with the hot water and hot air, simultaneously.

REFERENCES

[1] D.J.A. Beckman, *Solar Engineering of Thermal Processes*, 3rd ed, Wiley, New York, 2006.

[2] D. Chauhan, S. Agarwal and M.K. Suman, "Photovoltaic thermal system and their various aspects: A review," *International Journal of Scientific & Technology Research*, vol. 2, no. 9, pp. 79-88, 2013.

[3] T.T. Chow, W. He and J. Ji, "Hybrid photovoltaic thermosyphon water heating system for residential application," *Solar Energy*, vol. 80, no. 3, pp298–30, 2006.

[4] A. Ibrahim, M.Y. Othman, M.H. Ruslan, S. Mat and K. Sopian, "Recent advances in flat plate photovoltaic/thermal (PV/T) solar collectors," *Renewable and Sustainable Energy Reviews*, vol. 15, no. 1, pp. 352-365, 2011.

[5] M.A. Tabook, M.Y. Othman, K. Sopian and M.H. Ruslan, "A review paper on PV/T combination flat plate," *World Essays Journal,* vol. 1, no. 1, pp. 1-5, 2014.

[6] J.K. Tonui and Y. Tripanagnostopoulos, "Improved PV/T solar collectors with heat extraction by

forced or natural air circulation," *Renewable Energy*, vol. 32, no. 4, pp. 623-637, 2007.

[7] J.K. Tonui and Y. Tripanagnostopoulos, "Air-cooled PV/T solar collectors with low cost performance improvements," *Solar Energy*, vol. 81, no. 4, pp. 498–511, 2007.

[8] Y.B. Assoa, C. Menezo, G. Fraisse, R. Yezou and J. Brau, "Study of a new concept of photovoltaic-thermal hybrid collector", *Solar Energy*, vol. 81, no. 9, pp. 1132-1143, 2007.

Thermal stress effect on disc brake rotor for NGV vehicle

B. Baharin[1], M.Z. Akop[1,2,*], M.A. Salim[1,2], M.R. Mansor[1,2], A.M. Saad[1,2], M.A.M. Rosli[1,2], Y.M. Arifin[1,2], M.M. Tahir[1,2]

[1)] Faculty of Mechanical Engineering, Universiti Teknikal Malaysia Melaka, Hang Tuah Jaya, 76100 Durian Tunggal, Melaka, Malaysia
[2)] Centre for Advanced Research on Energy, Universiti Teknikal Malaysia Melaka, Hang Tuah Jaya, 76100 Durian Tunggal, Melaka, Malaysia

*Corresponding e-mail: zaid@utem.edu.my

Keywords: Straight vane; curved vane; temperature distribution; thermal stress

ABSTRACT - The concept of braking system may seem fairly obvious which is to stop the vehicle. Potential energy of the vehicle converts into heat due to frictional contact between the brake pads and the brake disc. The heat needs to be dissipated properly to the surrounding to avoid any failure from occurs. In order to get better understanding on temperature distribution and stress of the disc brake during braking operation, steady state and transient response are introduced. There are two types of disc brakes design being studied, which are straight vane and curved vane and the analysis is applied on normal passenger NGV vehicle. The findings of this research provide a useful design tool and improve the brake performance of disc brake system.

1. INTRODUCTION

A moving normal passenger vehicle powered by natural gas contains an amount of kinetic energy being transferred to the disc rotor during braking and simultaneously generates heat along the operations. To predict the temperature distribution and thermal stress of the disc brake, finite element analysis is applied via steady state and transient response method.

There are several types of brake simulation recommended to run the analysis [1-2]. Huang and Chen [1] suggested ten load cycles with a total time of 350 seconds to investigate the thermal stress and cooling performance of a brake. Each cycle consists of 6 seconds of braking from 100km/h and 29 seconds of idling (Figure 1).

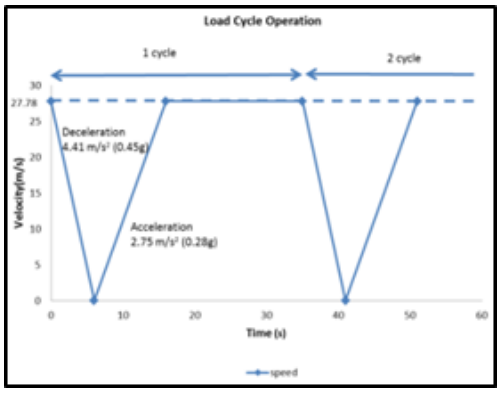

Figure 1 Huang and Chen [1] load cycles.

During the 6 seconds of braking, heat flux is applied on both disc braking surface (inboard and outboard). Force convection is applied for the rest of 29 seconds idling. Saiz et al. [2] proposed fourteen load cycles with total time of 550 seconds using Brembo (2014) fading test model. The test involved fourteen repeated braking events (Figure 2), with a constant deceleration. Besides, there will be also a recovery time or idling between two braking events. The initial velocity, V_i, is 160 km/h (44.44 m/s).

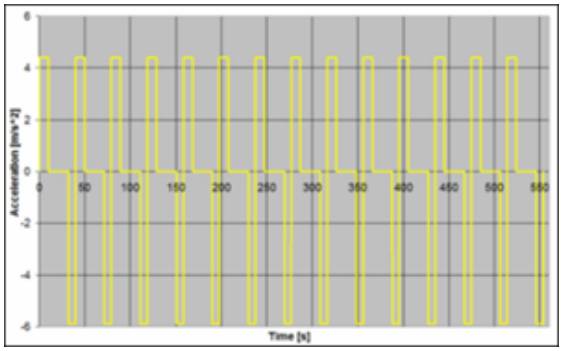

Figure 2 Saiz et al. [2] load cycles.

2. METHODOLOGY

The dimension of straight vane disc brake measured from normal passenger vehicle using coordinate measuring machine and digital calliper. The curved vane shares the same dimension except the vane is curved at an angle 150°. The dimension is then used to generate 3D model of disc brake using SOLIDWORKS for both type of disc brake. Since axis-symmetrical consideration, only a 120 fraction of disc brake for both type is used in this analysis. Both 3D models are then export to ANSYS software. CES Edupack (2013) is used to select the suitable grey cast iron which is EN GJL 200 grade for both disc brakes in this simulation.

This analysis requires input of the total energy absorbed by the front brake disc rotor during braking events. Therefore, normal passenger NGV vehicle is used as a test model to conduct the temperature distribution and thermal stress behaviour. In order to get better and reliable result the specific heat capacity, the thermal conductivity and the elastic modulus of the disc brake material are also included. All properties of air related to this analysis are based on the ambient air temperature condition (300°C). This project is carried out using Finite Element Analysis (FEA) software which is ANSYS.

In ANSYS temperature distribution simulation, both steady state and transient response share the same material engineering data except time setting. In thermal stress analysis, the body temperature obtained from transient response analysis is exported to transient structural simulation.

3. LOAD ANALYSIS

Due to the complexity of thermal load calculation, Belhocine et al. [3] had also list out several assumptions to be considered during the load analysis in order to obtain reliable results. Besides, Limpert [4], also has simplified the analysis by assuming the disc brake as lumped system while the heat transfer coefficient and the thermal properties are remaining constant throughout the analysis.

For this case study, ten load cycles is applied for both straight and curved vane [1]. According Janeesh et al. [5] claims that 13% of improvement of heat dissipation are recorded in curved vane design compared to straight vane. In this analysis, the 13% improvement is only considered to the conventional heat transfer coefficient on inner vane passage as shown in Table 1. The values obtained in Table 1 are used in ANSYS simulation in order to get the temperature distribution as well as the thermal stress.

Table 1 Disc brake properties.

	Type of vane	Straight	Curved
Heat flux (W/m^2)	Surface		
	Inboard	534,024.57	
	Outboard	488,089.45	
Convectional heat transfer coefficient ($W/m^2.°C$)	Inboard & Outboard	221.75	
	Outer Ring Surface	63.05	
	Inner Ring (Outer)	52.72	
	Inner Ring (Inner Upper)	51.22	
	Inner Ring (Inner Bottom)	53.18	
	Inner Vane Passage	134.67	152.18

4. RESULTS AND DISCUSSION

In steady state, thermal analysis, both disc brakes are subjected to heat flux on outboard and inboard surfaces continuously without stop. Although force convections are applied on inboard, outboard, outer ring, vane, inner ring (outer), inner ring (inner upper) and inner ring (inner bottom), the temperature keep on arising until it reaches a maximum of 1,385.5°C for straight vane and 1,328.6°C for curved vane. Curved vane recorded slightly lower temperature due to higher force convection at the inner vane passage. Due to continuous braking, both disc brakes temperature exceeded the melting point (1,130°C – 1,240°C) and maximum service temperature (350°C – 450°C).

For transient response, thermal analysis, ten load cycles are applied. Each cycle consists of 35 seconds, where 6 seconds of braking (heat flux is applied) and 29 seconds of idling (convection). The highest ever temperature recorded for straight vane and curved vane are 342.62°C and 339.13°C respectively. Since these values are below than the maximum service temperature of grey cast iron (EN GJL 200) which is 450°C, thus these temperatures are acceptable Figure 4.

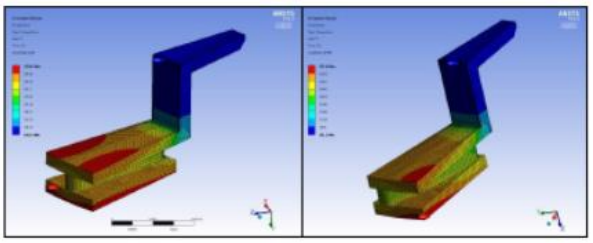

Figure 4 Transient response temperature.

The straight vane recorded 799.67 MPa for maximum stress after 350 seconds while curved vane shows a higher maximum stress of 937.26 MPa. The maximum stress occurs at the corner of the inner hat/hub section of the disc brake where the frictionless support is located. Although the stress recorded are higher than tensile strength of grey cast iron EN JL 200 which is 290 MPa, the results obtained show the values are still below the Young's Modulus value which is 120 GPa. Both disc brakes are still in elastic deformation region where it has the tendency to return to its original shape. The maximum deformation obtained for straight vane is 1.8583 mm while curved vane shows 1.8109 mm.

5. CONCLUSION

From this analysis, transient response is clearly the better choice in determining the temperature distribution and thermal stress. It tries to replicate the real-time condition of braking operations which is not available in steady state analysis. The results are below melting point and service temperature of the grey cast iron (EN GJL 200). Due to software and hardware limitation, the stress recorded are higher than tensile strength of grey cast iron but it is still in the elastic region which is still acceptable. From these findings, it shows that curved vane is generally better choice of disc brake for extreme driving while straight vane is for daily normal driving.

REFERENCES

[1] Y.M. Huang and S.H. Chen, "Analytical study of design parameters on cooling performance of a brake," *SAE Technical Paper,* pp. 1-10, 2006.

[2] C.B. Saiz, T. Ingrassia, V. Nigrelli and V. Ricotta, "Thermal stress analysis of different full and ventilated disc brakes," *Frattura ed Integrità Strutturale*, vol. 34, pp. 608-621, 2015.

[3] A. Belhocine, C.D. Cho, M. Nouby, Y.B. Yi and A.R. Abu Bakar, "Thermal analysis of both ventilated and full disc brake rotors with frictional heat generation," *Applied and Computational Mechanics,* vol. 8, pp. 5-24, 2014.

[4] R. Limpert, "Cooling analysis of disc brake rotors," *SAE Technical Paper*, pp. 1-8, 1975.

[5] M.M. Janeesh, V. Arunkumar, C. Pradeepkumar and A.S. Ramkumar, "Analysis of cooling characteristics in automotive disc brake," *International Journal of Engineering Science Invention Research & Development*; vol. II, no. III, pp. 144-149, 2015.

Boundary layer flow of Jeffrey fluid over a stretching sheet with convective boundary conditions: Application in polymer processing

S.M. Zokri[1], N.S. Arifin[1], L.A. Aziz[1], M.K.A. Mohamed[1], M.Z. Salleh[1,*], A.R.M. Kasim[1], N.F. Mohammad[2]

[1)] Applied & Industrial Mathematics Research Group, Faculty of Industrial Science & Technology, Universiti Malaysia Pahang, 26300 Kuantan, Pahang, Malaysia
[2)] Department of Computational and Theoretical Sciences, Kulliyyah of Science, International Islamic University Malaysia, 25200 Kuantan, Pahang, Malaysia

[*]Corresponding e-mail: zuki@ump.edu.my

Keywords: Jeffrey fluid; stretching sheet; polymer processing

ABSTRACT – In this study, the boundary layer flow and heat transfer of Jeffrey fluid past a stretching sheet with convective boundary conditions is discussed. The governing system of partial differential equations is transformed into ordinary differential equations, which are then solved numerically via the Keller-box method encoded in MATLAB software. The numerical results for the temperature are obtained for various values of Prandtl and Biot number. The computation shows that as Prandtl number increases, the temperature profile is decreases.

1. INTRODUCTION

The important process of polymer processing is thermoplastic materials, that is extrusion and injection moulding. The single and twin extruders are used for melting and pumping the polymers as well as for die extrusion to produce film, sheet, pipe, tubing, profiles and fibres. The thermoplastics are usually processed in the molten state, where the solution of polymers are highly viscous, non-Newtonian and viscoelastic natures. The thermal diffusivity of most polymers is in the order of 10^{-7} m^2/s, which is about 1000 times less than the value for copper [1]. Hence, it is necessary to split the polymer into thin layers and this accounts to the main reasons for the increased use of polymers in recent years.

In this study, the Jeffrey fluid is chosen as it can represent the characteristics of solution of polymers. The problems associated with boundary layer flow due to a stretching sheet in Jeffrey fluid has begun to fascinate many researchers. For instance, Qasim [2] explored the effect of heat source/heat sink over stretching sheet in Jeffrey fluid while the effect of entropy generation and viscous dissipation has been studied by Dalir [3]. Very recently, Al-Sharifi et al. [4] studied the Jeffrey fluid with the convective boundary condition.

Therefore, the present work will focus on the convection boundary layer flow past a stretching sheet immersed in Jeffrey fluid with convective boundary condition. The scope of this study is only limited to the mathematical computation.

2. METHODOLOGY

2.1 Overview of physical model

A steady two-dimensional flow over a stretching sheet immersed in an incompressible Jeffrey fluid of ambient temperature, T_∞ is considered. The rectangular Cartesian coordinates (x, y) are used in which $x-$ and $y-$ axes are measured parallel to the plate and normal to it, respectively and the fluid occupies the region $y \geq 0$ as shown in Figure 1.

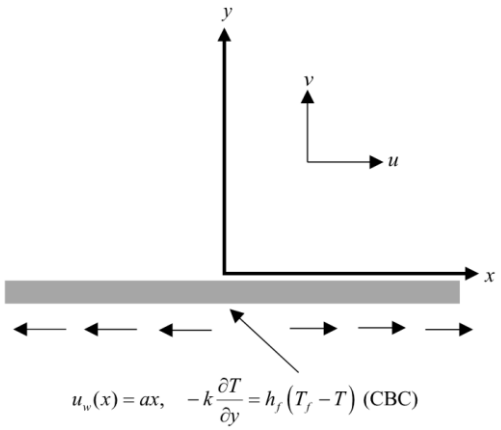

Figure 1 Physical model of the coordinate system.

2.2 Governing equation

Under the assumption that the boundary layer is valid, the continuity, momentum and energy equations can be written as follows

$$\frac{\partial u}{\partial x}+\frac{\partial v}{\partial y}=0, \tag{1}$$

$$u\frac{\partial u}{\partial x}+v\frac{\partial v}{\partial y}=\frac{\nu}{1+\lambda}\left[\frac{\partial^2 u}{\partial y^2}+\lambda_1\left(\begin{array}{l} u\dfrac{\partial^3 u}{\partial x\partial y^2}+v\dfrac{\partial^3 u}{\partial y^3}- \\ \dfrac{\partial u}{\partial x}\dfrac{\partial^2 u}{\partial y^2}+\dfrac{\partial u}{\partial y}\dfrac{\partial^2 u}{\partial x\partial y}\end{array}\right)\right] \tag{2}$$

$$u\frac{\partial T}{\partial x}+v\frac{\partial T}{\partial y}=\alpha\frac{\partial^2 T}{\partial y^2}, \tag{3}$$

subject to the boundary conditions

$$u=u_w(x),\ v=0,\ -k\frac{\partial T}{\partial y}=h_f\left(T_f-T\right)\ \text{at}\ y=0$$
$$u\to 0,\ v\to 0,\ T\to T_\infty\ \text{as}\ y\to\infty \tag{4}$$

where $u_w(x)=ax$ is the stretching velocity with a being the positive constant, while u and v are the velocity

components along the $x-$ and $y-$directions, respectively. Further, μ is the dynamic viscosity, v is the kinematic viscosity, λ is the ratio of relaxation and retardation times, λ_1 is the relaxation time, α is the thermal diffusivity, T is the local temperature, ρ is the fluid density, T_f is the hot fluid temperature, k is the thermal conductivity and h_f is the heat transfer coefficient. Introducing the similarity transformation variables and stream function

$$\eta = \left(a/v\right)^{1/2} y,\ \psi = (av)^{1/2} x f(\eta),\ \theta(\eta) = \frac{(T-T_\infty)}{(T_f - T_\infty)}$$
$$u = \frac{\partial \psi}{\partial y},\ v = -\frac{\partial \psi}{\partial x}. \quad (5)$$

Substituting Eq. (5) into Eqs. (1)-(3) and boundary conditions (4), the following nonlinear ordinary differential equations are obtained

$$f''' + (1+\lambda)(ff'' - f'^2) + \lambda_2 (f''^2 - ff^{iv}) = 0 \quad (6)$$

$$\theta'' + \Pr f\theta' = 0 \quad (7)$$

with boundary conditions

$$f(0) = 0,\ f'(0) = 1,\ \theta'(0) = -Bi(1-\theta(0)) \text{ at } y = 0$$
$$f'(\infty) \to 0,\ f''(\infty) \to 0,\ \theta(\infty) \to 0 \text{ as } y \to \infty \quad (8)$$

where $\lambda_2 = \lambda_1 a$ and $Bi = \left(h_f/k\right)\sqrt{v/a}$ are Deborah and Biot number, respectively.

2.3 Keller-box method

Eqs. (6) and (7) with boundary condition (4) are solved using the Keller-box method which comprises the following steps:

a. Reduce the non-linear partial differential equations into first order system
b. Finite Difference Discretization
c. Linearization by using the Newton's method
d. Solve the linear system by the block tridiagonal elimination technique

3. RESULTS AND DISCUSSION

Table 1 shows the comparison values of skin friction coefficient $f''(0)$ with existing publication reported by Dalir [3]. The results exhibit an excellent agreement with existing work.

From Fig. 2, an increase in Pr leads to a decrease in temperature profiles. Physically, higher values of Pr will lessen the conduction while enhancing pure convection (transfer of heat through unit area), thereby diminishing the boundary layer thickness and thus, increasing the heat transfer rate. In Fig. 3, it is noticed that the stronger convective heating at the sheet allows the thermal effect to penetrate deeper into the fluid. This results in larger temperature as well as thicken the thermal boundary layer.

4. CONCLUSION

The results obtained in the present study are significant in polymer processing. This is because, the process involves the transfer of heat that is very useful to predict the optimum output in the production of polymer components.

Table 1 Comparison between the present solutions and previous published results when $\lambda = 0.2$.

	$f''(0)$	
λ_2	**Dalir [3]**	**Present**
0.0	-1.09544512	-1.09544525
0.2	-1.00000000	-1.00000037
0.4	-0.92582010	-0.92582035
0.6	-0.86602540	-0.86602540
0.8	-0.81649658	-0.81649649
1.0	-0.77459667	-0.77459676

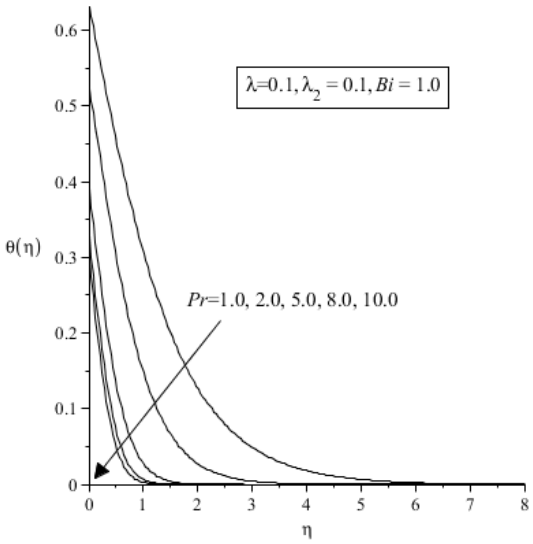

Figure 2 Temperature profile $\theta(\eta)$ versus Pr.

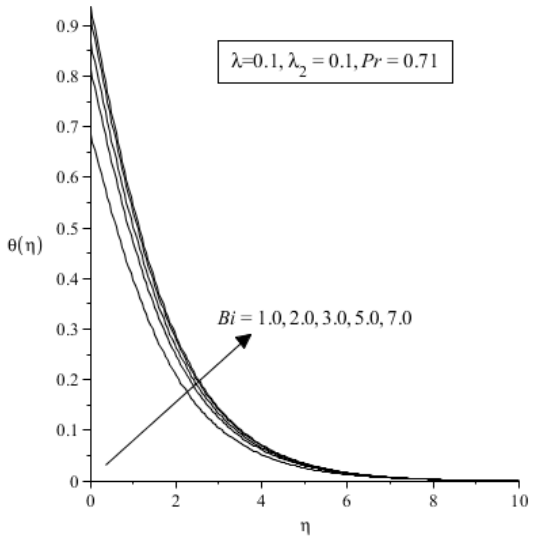

Figure 3 Temperature profile $\theta(\eta)$ versus Bi.

ACKNOWLEDGEMENT

The authors gratefully acknowledge the financial supports (RDU150101 & RDU160330) received from Universiti Malaysia Pahang.

REFERENCES

[1] K.E. George, "2 - Non-Newtonian fluid mechanics and polymer rheology," in *Advances in Polymer Processing*, Woodhead Publishing; 2009.

[2] M. Qasim, "Heat and mass transfer in a Jeffrey fluid over a stretching sheet with heat source/sink," *Alexandria Engineering Journal,* vol. 52, pp. 571-575, no. 4, 2013.

[3] N. Dalir, "Numerical study of entropy generation for forced convection flow and heat transfer of a Jeffrey fluid over a stretching sheet," *Alexandria Engineering Journal,* vol. 53, pp. 769-778, no. 4, 2014.

[4] H.A.M. Al-Sharifi, A.R.M. Kasim, M.Z. Salleh, N.M. Sarif, N.F. Mohammad, S. Shafie and A. Ali, "Influence of slip velocity on convective boundary layer flow of Jeffrey fluid under convective boundary conditions," *ARPN Journal of Engineering and Applied Sciences,* vol. 11, no. 18, 2016.

Mathematical modelling on convective boundary layer of non-Newtonian micropolar viscoelastic fluid

L.A. Aziz[1,*], N.S. Arifin[1], S.M. Zokri[1], A.R.M. Kasim[1], M.Z. Salleh[1], I. Waini[2], S. Shafie[3]

[1)] Applied & Industrial Mathematics Research Group, Faculty of Industrial Sciences & Technology, Universiti Malaysia Pahang, 26300 Kuantan, Pahang, Malaysia
[2)] Faculty of Engineering Technology, Universiti Teknikal Malaysia Melaka, Hang Tuah Jaya, 76100 Durian Tunggal, Melaka, Malaysia
[3)] Faculty of Science, Universiti Teknologi Malaysia, 81310 Johor, Malaysia

[*]Corresponding e-mail: laila@ump.edu.my

Keywords: Viscoelastic micropolar; circular cylinder; mixed convection

ABSTRACT – This article presents the mixed convection boundary layer flow over a circular cylinder placed in a viscoelastic micropolar fluid with surface heat flux. The governing boundary layer equations are transformed into non-dimensional form by using appropriate dimensionless variables. Then, the resulting equations are transformed into similarity equations and solved using an implicit finite difference scheme known as the Keller box method. For validation purpose, the current results are compared to previous study. With congruent results from both study, authors are convinced that the proposed model is reliable.

1. INTRODUCTION

Viscoelastic is a renowned type of fluid in industrial-manufacturing processes and engineering field with practicality in petroleum drilling, manufacturing of foods and paper, as well as reducing frictional drag on the hulls of ships and submarines. The study of the flow of viscoelastic fluid has sparked interests in many researchers due to its special ability to deform semi-permanently. However, in the existing models of viscoelastic fluids (refer [1-3]), the presence of rigid, randomly oriented suspended particles are neglected. Considering that the presence of the particles in the fluid might affect the behavior of the flow and heat transfer, therefore, this article will propose a new model of viscoelastic micropolar fluid.

According to the model proposed by Eringen in [4], micropolar fluids is a type of fluid consisting of rigid, randomly oriented (or spherical) particles suspended in a viscous medium which is particularly useful to model fluids with presence of dust and smoke, especially in gas. Hence, viscoelastic micropolar fluid can be defined as fluid with suspended particles that displays viscous and elastic characteristics.

In this study, the outcomes of the numerical solutions of the fluid flow of viscoelastic micropolar model on the outer of a circular cylinder will be presented.

2. METHODOLOGY

2.1 Mathematical formulation

Figure 1 illustrates the physical geometry of the problem and the corresponding coordinate system.

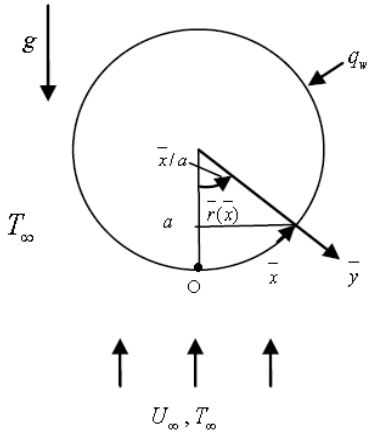

Figure 1 Physical model and coordinate system.

Under the assumptions that the Boussinesq and boundary layer approximations are valid, the dimensional equations governing the mixed convection boundary layer flow are

Continuity equation:

$$\frac{\partial \bar{u}}{\partial \bar{x}} + \frac{\partial \bar{v}}{\partial \bar{y}} = 0 \tag{1}$$

Momentum equation:

$$\bar{u}\frac{\partial \bar{u}}{\partial \bar{x}} + \bar{v}\frac{\partial \bar{u}}{\partial \bar{y}} = \bar{u}_e\frac{\partial \bar{u}_e}{\partial \bar{x}} + \left(\frac{\mu+\kappa}{\rho}\right)\frac{\partial^2 \bar{u}}{\partial \bar{y}^2} + K_0\left(\frac{\partial}{\partial \bar{x}}\left(\bar{u}\frac{\partial^2 \bar{u}}{\partial \bar{y}^2}\right) + \bar{v}\frac{\partial^3 \bar{u}}{\partial \bar{y}^3} - \frac{\partial \bar{u}}{\partial \bar{y}}\frac{\partial^2 \bar{u}}{\partial \bar{x}\partial \bar{y}}\right)$$
$$- g\beta(T - T_\infty)\sin\left(\frac{\bar{x}}{a}\right) + \frac{\kappa}{\rho}\frac{\partial \bar{H}}{\partial \bar{y}} \tag{2}$$

Energy equation:

$$\bar{u}\frac{\partial T}{\partial \bar{x}} + \bar{v}\frac{\partial T}{\partial \bar{y}} = \alpha\frac{\partial^2 T}{\partial \bar{y}^2} \tag{3}$$

Micropolar equation:

$$\rho j\left(\bar{u}\frac{\partial \bar{H}}{\partial \bar{x}}+\bar{v}\frac{\partial \bar{H}}{\partial \bar{y}}\right)=-\kappa\left(2\bar{H}+\frac{\partial \bar{u}}{\partial \bar{y}}\right)+\gamma\frac{\partial^2 \bar{H}}{\partial \bar{y}^2} \quad (4)$$

subject to the boundary conditions,

$$\bar{u}=\bar{v}=0, \quad \frac{\partial T}{\partial \bar{y}}=-\frac{q_w}{k}, \quad \bar{H}=n\frac{\partial \bar{u}}{\partial \bar{y}} \quad \text{on} \quad \bar{y}=0,$$

$$\bar{u}=\bar{u}_e(x), \quad \frac{\partial \bar{u}}{\partial \bar{y}}=0, \quad T=T_\infty, \ \bar{H}=0 \quad \text{as} \quad y\to\infty \quad (5)$$

2.2 Numerical computation

The above equations are transformed to non-dimensional form by using appropriate dimensionless variables to reduce the complexity of the equations. Then, the non-dimensional governing equations are transformed into similarity equations and solved using an implicit finite difference scheme known as the Keller box method using Fortran programming.

3. RESULTS AND DISCUSSION

In order to validate the reliability of the proposed model, the numerical solution obtained is compared with the existing model by Merkin [5] which also investigated the mixed convection flow on a horizontal circular cylinder. The present model is convertible to the existing model which considers the case of Newtonian fluid by neglecting the viscoelastic and micropolar parameter. Upon comparison with the published result on the values of skin fraction and heat transfer at different values of mixed convection parameter, it is observed that both results are highly in agreement.

Table 1 Comparison for the values of $f''(0)$ and $-\theta'(0)$ with published results.

λ	Merkin [5]		Present	
	$f''(0)$	$-\theta'(0)$	$f''(0)$	$-\theta'(0)$
-1.9	-0.09987	0.38467	-0.099929	0.384652
-1.8	0.01950	0.40993	0.019467	0.409934
-1.6	0.20923	0.44409	0.209196	0.444091
-1.4	0.36982	0.46907	0.369794	0.469064
-1.2	0.51460	0.48935	0.514586	0.489351
-1.0	0.64886	0.50667	0.648916	0.506689
-0.8	0.77554	0.52193	0.775596	0.521961
-0.6	0.89627	0.53566	0.896256	0.535678
-0.4	1.01219	0.54818	1.012254	0.548210
-0.2	1.12410	0.55973	1.124066	0.559742
0.0	1.23259	0.57047	1.232658	0.570492
0.2	1.33810	0.58052	1.338181	0.580548
0.4	1.44100	0.58999	1.439679	0.589864
0.6	1.54158	0.59895	1.541523	0.598964
0.8	1.64007	0.60747	1.640159	0.607493
1.0	1.73666	0.61559	1.736780	0.615613
1.4	1.92482	0.63079	1.922781	0.630629
1.8	2.10711	0.64484	2.106987	0.644849
2.2	2.28432	0.65792	2.281646	0.657725
3.0	2.62587	0.68173	2.622574	0.681504
5.0	3.42296	0.73151	3.422668	0.731512
8.0	4.51480	0.79017	4.506890	0.789785
10.0	5.19484	0.82264	5.195332	0.822686

After validating the reliability of the results, this problem is then extended to find the temperature and velocity distributions with selection of viscoelastic parameter values. Those results have a significant role as they help to determine what type of materials are the most compatible for certain processes where heat transfer is involved.

4. CONCLUSION

Based on the proposed mathematical model, we can conclude that the viscoelastic micropolar model is an ideal fit to represent the flow of viscoelastic fluid with suspended particles.

The flow of blood in our body is a perfect example to illustrate this study. Blood is a viscoelastic fluid as it is both viscous and elastic and it also consists of suspension of platelets, red blood cells, and white blood cells consisting of neutrophils, lymphocytes and monocytes which are suspended particles. The flow of blood in our body is affected by natural causes including gravity and also external forces such as physical activities. As for the geometrical shape related to this study, our body also consists of cylindrical blood vessels. However, experimental study is necessary to ascertain that our result is applicable to this case.

Overall, the existence of the proposed model will improve the accuracy of the existing models where the presence of such particles in fluid are overlooked. The finding from this study could benefit various sectors including industrial processes and medical field.

ACKNOWLEDGEMET

The authors would like to express our gratitude for financial support received from Universiti Malaysia Pahang (UMP) for RDU160330 and RDU161106.

REFERENCES

[1] A. Kasim and S. Shafie, "Mixed convection boundary layer of a viscoelastic fluid past a circular cylinder with constant heat flux," in *Proceedings of the 1st Regional Conference on Applied and Engineering Mathematics*, 2010, pp. 124-129.

[2] H. Ahmad, T. Javed and A. Ghaffari, "Radiation effect on mixed convection boundary layer flow of a viscoelastic fluid over a horizontal circular cylinder with constant heat flux," *Journal of Applied Fluid Mechanics,* vol. 9, pp. 1167-1174, 2016.

[3] A.R.M. Kasim, N.F. Mohammad and S. Shafie, "Effect of heat generation on free convection boundary layer flow of a viscoelastic fluid past a horizontal circular cylinder with constant surface heat flux," *AIP Conference Proceedings,* vol. 1450, pp. 286-292, 2012.

[4] A.C. Eringen, "Simple microfluids," *International Journal of Engineering Science,* vol. 2, pp. 205-217, 1964.

[5] J. Merkin, "Mixed Convection from a horizontal circular cylinder " *International Journal of Heat and Mass Transfer,* vol. 20, pp. 73-77, 1977.

Mathematical modeling on aligned magnetic field of two-phase dusty Casson fluid

N.S. Arifin[1], S.M. Zokri[1], L.A. Aziz[1], A.R.M. Kasim[1,*], M.Z. Salleh[1], N.F. Mohammad[2]

[1)] Applied & Industrial Mathematics Research Group, Faculty of Industrial Sciences & Technology, Universiti Malaysia Pahang, 26300 UMP Kuantan, Pahang, Malaysia
[2)] Department of Computational and Theoretical Sciences, Kulliyyah of Sciences, International Islamic University Malaysia, 25200 Kuantan, Pahang, Malaysia

[*]Corresponding e-mail: rahmanmohd@ump.edu.my

Keywords: Aligned magnetic field; two-phase flow; dusty Casson fluid

ABSTRACT – The influence of aligned magnetic field on the two-phase flow of Casson fluid and dust particle with heat transfer over a stretching sheet subjected to convective boundary conditions (CBC) is analysed. The governing equations are transformed into ordinary differential equations by employing similarity transformation which then solved numerically by Runge-Kutta Fehlberg fourth-fifth method (RKF45). The effects of aligned angle and fluid particle interaction parameter are presented graphically for both phases by fixing several physical parameters. It has been found that aligned angle strengthens the magnetic field and led to decrease the velocity profile for both phases.

1. INTRODUCTION

A considerable amount of effort has been made on the topic of non-Newtonian fluid due to its practical applications, for instance in manufacture of plastic film and in extrusion of polymer sheet from a die. Numerous non-Newtonian fluid models have been developed to exhibit its physical properties. One of them is Casson fluid which possesses the interactive behaviour of solid and liquid phases. Such fluids are honey, jelly, tomato sauce and concentrated fruit juices. Human blood which contained protein, fibrinogen and globulin in an aqueous base plasma also can be categorized as Casson fluid [1].

The two-phase flow of solid spherical particles is scattered in a fluid and can be observe in sediments, environment pollution, centrifugal separation of particle and blood rheology. Moreover the flow in the channel of magnetohydrodynamic (MHD) generators is affected by the accumulation of ash or soot [2]. The two-phase fluid model is used to analyse the alkaline anion exchange membranes (AAEMs) conductivity and a numerical simulation is carried out for blood purification auto-transfusion dialysis hybrid devices [3,4].

2. METHODOLOGY

2.1 Mathematical formulation

The boundary layer flow of dusty Casson fluid with velocity $u_w(x) = ax$ is considered. An aligned magnetic field with an acute angle α_1 is applied to the flow as shown in Figure 1. Supposed, the dust particles are in spherical shape, uniform size and number density of these are taken as constant throughout the flow.

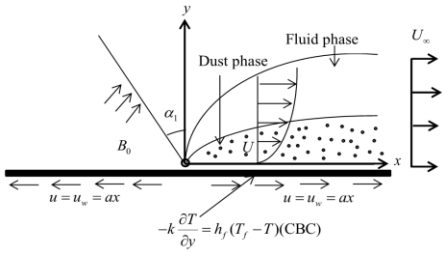

Figure 1 Flow configuration.

Under Boussinesq and boundary layer approximations, the governing equations can be written as two part:

Fluid phase:

$$\frac{\partial u}{\partial x} + \frac{\partial v}{\partial y} = 0, \tag{1}$$

$$\rho_\infty \left(u\frac{\partial u}{\partial x} + v\frac{\partial u}{\partial y} \right) = \mu\left(1 + \frac{1}{A}\right)\left(\frac{\partial^2 u}{\partial y^2}\right) + \frac{\rho_p}{\tau}(u_p - u) - \sigma u B_0{}^2 \sin^2\alpha_1, \tag{2}$$

$$\rho_\infty c_p \left(u\frac{\partial T}{\partial x} + v\frac{\partial T}{\partial y} \right) = k\left(\frac{\partial^2 u}{\partial y^2}\right) + \frac{\rho_p c_s}{\gamma_T}(T_p - T), \tag{3}$$

Dust phase:

$$\frac{\partial u_p}{\partial x} + \frac{\partial u_p}{\partial y} = 0, \tag{4}$$

$$\rho_p \left(u_p\frac{\partial u_p}{\partial x} + v_p\frac{\partial u_p}{\partial y} \right) = \frac{\rho_p}{\tau}(u - u_p), \tag{5}$$

$$\rho_p c_s \left(u_p\frac{\partial T_p}{\partial x} + v_p\frac{\partial T_p}{\partial y} \right) = -\frac{\rho_p c_s}{\gamma_T}(T_p - T). \tag{6}$$

The boundary conditions associated with the model are

$$\begin{aligned} &u = u_w(x), v = 0, -k\left(\partial T/\partial y\right) = h_f\left(T_f - T\right) \text{ at } y = 0 \\ &u \to 0, u_p \to 0, v_p \to v, T \to T_\infty, T_p \to T_\infty \text{ at } y \to \infty \end{aligned} \tag{7}$$

In order to reduce the complexity of Equation (1)-(7), the similarity transformations are introduced:

$$u = axf'(\eta), v = -\sqrt{av}\, f(\eta), \eta = \sqrt{\frac{a}{v}}y, u_p = axF'(\eta),$$
$$v_p = -\sqrt{av}F(\eta), \theta(\eta) = \frac{T - T_\infty}{T_f - T_\infty}, \theta_p(\eta) = \frac{T_p - T_\infty}{T_f - T_\infty}, \quad (8)$$

Equations (1)-(7) now reduced to

$$\left(1+\frac{1}{B}\right) f'''(\eta) + f(\eta) f''(\eta) - [f'(\eta)]^2 + \beta N[F'(\eta) - f'(\eta)] - Mf'(\eta)\sin^2\alpha_1 = 0, \quad (9)$$

$$\theta''(\eta) + \Pr f(\eta)\theta'(\eta) + \frac{2}{3}\beta N[\theta_p(\eta) - \theta(\eta)] = 0, \quad (10)$$

$$[F'(\eta)]^2 - F(\eta)F''(\eta) + \beta[F'(\eta) - f'(\eta)] = 0, \quad (11)$$

$$\theta_p'(\eta)F(\eta) + \frac{2}{3}\frac{\beta}{\lambda \Pr}[\theta_p(\eta) - \theta(\eta)] = 0, \quad (12)$$

and boundary conditions becomes

$$f(0) = 0, f'(0) = 1, \theta'(0) = -\gamma(1 - \theta(0)) \text{ at } \eta = 0$$
$$f'(\eta) \to 0, F'(\eta) \to 0, \theta(\eta) \to 0, \quad (13)$$
$$\theta_p(\eta) \to 0 \qquad \text{at } \eta \to \infty$$

2.2 Numerical computation

In order to solve the Equations (9)-(13), the Runge-Kutta Fehlberg fourth-fifth method (RKF45) in Maple software is applied. The boundary layer thickness of $\eta_\infty = 5$ is selected for boundary conditions to fully satisfied.

3. RESULTS AND DISCUSSION

For validation purposes, the present results are compared with existing outcome in literature for limiting case and it shows a very good agreement (see Table 1) when $\Pr = 7, M = \alpha_1 = N = \beta = 0, B = \lambda \to \infty$. Therefore, the authors confident the present numerical results presented in this reports are acceptable.

Figures 2 and 3 illustrated the influences of aligned angle α_1 and fluid particle interaction parameter β on velocity and temperature profiles respectively. It is observed that α_1 is the decreasing function of velocity profile for both phases due to the development of magnetic field. The temperature profile for fluid phase is decrease while increase for dust phase with the larger β.

Table 1 Comparison for the values of $-\theta'(0)$ with previously published results.

γ	Sarif et al. [5]	Present
0.05	0.02571	0.02571
0.1	0.05012	0.05012
0.7	0.26976	0.26976
1.0	0.34544	0.34544

4. CONCLUSION

The investigations of two-phase flow of fluids having dust particle is significant since the accumulation of dust particle near the wall could reduce the performance of certain engineering devices. The aligned angle and fluid-interaction parameter have a significantly influenced the velocity and temperature profiles respectively for both phases. Indeed, this understanding can be used to enhance the fluid flow and heat transfer processes.

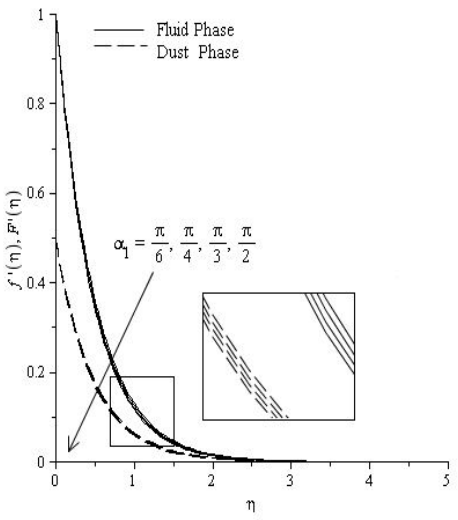

Figure 2 The velocity profile for variation of α_1.

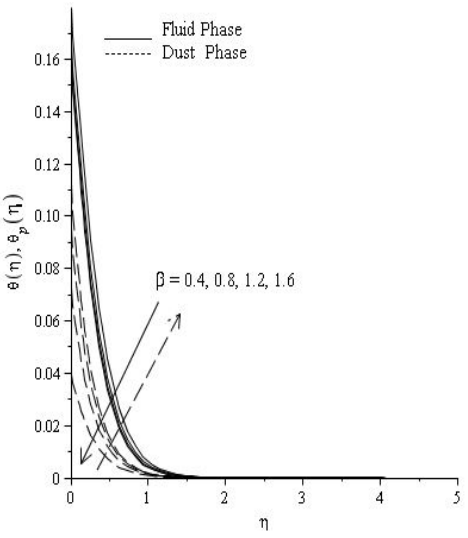

Figure 3 The temperature profile for variation of β.

ACKNOWLEDGMENT

The authors gratefully acknowledge the financial support received in the form of fundamental research grants (FGRS) fund from the Ministry of Higher Educational, Malaysia, RDU 150101 and Universiti Malaysia Pahang (UMP) for RDU 160330.

REFERENCES

[1] S. Mukhopadhyay, P.R. De, K. Bhattacharyya and G. Layek, "Casson fluid flow over an unsteady stretching surface," *Ain Shams Engineering Journal*, vol. 4. no. 4, pp. 933-938, 2013.

[2] K. Gopinath, "Viscous Dusty Fluid Flow with Constant Velocity Magnitude," *Electronic Journal of Theoretical Physics*, vol. 5, no. 17, pp. 237-252, 2008.

[3] K.N. Grew and W.K. Chiu, "A dusty fluid model for predicting hydroxyl anion conductivity in alkaline anion exchange membranes," *Journal of the electrochemical Society*, vol. 157, no. 3, pp. B327-B337, 2010.

[4] O.A. Beg, B. Vasu, T. Sochi and V. Prasad, "Keller Box and Smoothed Particle Hydrodynamic Numerical Simulation of Two-Phase Transport in Blood Purification Auto-Transfusion Dialysis Hybrid Device with Stokes and Darcy Number Effects," *Journal of Advanced Biotechnology and Bioengineering*, vol. 1, no. 2, pp. 80-100, 2013.

[5] N. Sarif, M. Salleh and R. Nazar, "Boundary layer flow and heat transfer over a stretching sheet with convective boundary conditions," in *AIP Conference Proceedings*, 2013, pp. 420-425.